https://doi.org/10.5194/essd-2026-557
Preprint. Discussion started: 10 September 2026

Earth System Science Data Discussions
Open Access

The ATMOSFER campaign: synergistic observations for the preparation of the ESA FORUM mission.

Mélanie Ghysels[1], Luca Palchetti[2], Silvia Viciani[2], Claudio Belotti[2], Marco Barucci[2], Gwenaël Berthet[5], Elizabeth Asher[6,7], Emrys Hall[6], Alex Fritz[6,7], Armin Afchine[8], Christian Rolf[8], Thomas Kuhn[9], Chris Stopford[14], Alain Hauchecorne[1], Nadir Amarouche[10], Georges Durry[11], Jean-Christophe Samake[10], Lars Kalnajs[12], Terry Deshler[12,13], Samuele Del Bianco[3], Paolo Pettinari[4]

[1] LATMOS/IPSL, Sorbonne Université, UVSQ, CNRS, Paris, 75252, France
[2] Consiglio Nazionale delle Ricerche, National Institute of Optics, Sesto Fiorentino, 50019, Italy
[3] Consiglio Nazionale delle Ricerche, Institute of Applied Physics "Nello Carrara", Sesto Fiorentino, 50019, Italy
[4] Consiglio Nazionale delle Ricerche, Institute for Atmospheric Sciences and Climate, 40129 Bologna, Italy
[5] Laboratoire de Physique et Chimie de l'Environnement et de l'Espace, CNRS UMR 7328, Université d'Orléans, Orléans, France
[6] NOAA Global Monitoring Laboratory, 325 Broadway R/GML1, Boulder, CO 80305, USA.
[7] Cooperative Institute for Research in Environmental Sciences, University of Colorado Boulder, Boulder, CO, United States
[8] Forschungszentrum Jülich GmbH, Institute of Climate and Energy Systems 4 – Stratosphere, 52425 Jülich, Germany
[9] Luleå University of Technology, Department of Computer Science, Electrical and Space Engineering, Kiruna, Sweden
[10] INSU Division Technique, CNRS, Gif-sur-Yvette, France
[11] LEATP, Université de Reims Champagne Ardenne, Reims, FRANCE
[12] Laboratory for Atmospheric and Space Physics (LASP), University of Colorado Boulder, Boulder, CO, USA.
[13] Department of Atmospheric Science, University of Wyoming, Laramie, WY, USA.
[14] Particle Instruments & Diagnostics; School of Physics, Engineering, & Computer Science; University of Hertfordshire, UK.

Correspondence to: Melanie Ghysels (melanie.ghysels-dubois@latmos.ipsl.fr)

Abstract. The balloon-borne ATMOSFER campaign, supported by CNES, was held in Kiruna in June 2024. This campaign involved lightweight hygrometers (Pico-Light H_2O, NOAA GML frost point hygrometer, EN-SCI Cryogenic frost point hygrometer), optical particle counters and ice crystal imager (POPS, LOAC v1.5, LPC and NIXE-B), ozone sondes and the airborne demonstrator of the future ESA FORUM mission developed by CNR-INO (FIRMOS-B instrument). The instruments have been flown aboard Zero Pressure Balloon (ZPB) and small weather balloons (RS) by CNES and the scientific teams. The synergistic observations aboard stratospheric balloons captured the signature of multiple influences which are useful for preparation activities of the ESA FORUM mission. The measurements revealed stratospheric intrusions of sub-tropical air, the presence of upper tropospheric ice cirrus clouds and aerosol layers of small particles potentially originating from volcanic eruption (between 15 and 17 km of altitude) and forest fires (near the polar cold point tropopause), which will influence the vertical profile retrievals from FIRMOS-B radiances and provide interesting features for radiative closure studies. This article aims to give an overview of the observation potential of the campaign for further studies in the frame of the ESA FORUM mission. The datasets are publicly available in the HEMERA datacenter (https://data.hemera-h2020.eu/atmospheric-balloon-experiments/#/).

https://doi.org/10.5194/essd-2026-557
Preprint. Discussion started: 10 September 2026

1 Introduction

The stratospheric water vapor global warming feedback has recently been estimated to be about $+0.3 W/m^2.K^{-1}$ of temperature change in the upper troposphere (Dessler, 2013; Dessler et al., 2014) with variability related to model selection (Banerjee et al., 2019). It is suspected that water vapor feedback is especially efficient near the tropopause, but large uncertainties remain. Stratospheric water vapor variability also substantially affects the surface radiation balance (Banerjee et al., 2019; Dessler et al., 2013; Nowack et al., 2023; Solomon et al., 2010). Charlesworth et al. (2023) shows that the atmospheric circulation in the troposphere and in the stratosphere is highly sensitive to the lowermost stratosphere water vapor via radiation and associated local temperature changes, leading to a first order effect on atmospheric circulation. Unlike for carbon dioxide, an extensive program is missing for the monitoring of long-term changes in upper tropospheric and lower stratospheric (UTLS) water vapor (Müller et al., 2016). Similarly, cloud radiative feedback remains the largest source of uncertainty in global climate models. The radiative impact of water in the TTL (Tropical Tropopause Layer) depends on its phase since there are differences in the infrared absorption between water vapor and ice crystals. Cirrus clouds play a critical role in the climate system and are a major source of uncertainty in our understanding of radiative balance.

Studies based on long-term balloon-borne measurements, satellite time series and models have tried to estimate a trend of stratospheric water vapor. Studies such as (Oltmans et al., 2000; Rosenlof et al., 2001) have shown an increase of about ~0.6 to 1 % per year in the period from 1980 and 2000 (Hurst et al., 2011b), with variabilities in latitude and altitude (Hegglin et al., 2014). Recent studies (Konopka et al., 2022; Tao et al., 2023) have shown a variability in the trends with time, with differences between both hemispheres. To date, no mean trend has clearly been identified. Such estimation remains challenging regarding the difficulty to accurately probe UTLS water vapor but also due to the limited spatial and temporal coverage of observations. While the processes driving stratospheric water vapor variability have been identified, their relative contribution in the modulation of the total mass flux entry remains undetermined. In addition, severe model biases regarding transport of water vapor across the tropopause and through the stratosphere pose a long-standing challenge to climate modeling (Charlesworth et al., 2023; Eyring et al., 2006; Keeble et al., 2021). Such models present a large wet bias in the lowermost stratosphere, where the radiation is most sensitive to water vapor changes and causes associated temperature biases.

The upcoming FORUM (Far-infrared Outgoing Radiation Understanding and Monitoring) mission of ESA (European Space Agency) will provide insights by measuring the Far Infrared (FIR) portion of the Earth's outgoing longwave radiation (OLR) from space. This wavelength region is highly sensitive to upper tropospheric water vapor and to cirrus clouds. The ATMOSFER campaign involved lightweight atmospheric hygrometers (Pico-Light H_2O, NOAA GML frost point hygrometer, cryogenic frost point hygrometer), optical particle counters (POPS, LOAC v1.5, LPC and NIXE-B), ice crystals imager (NIXE-B), ozone sondes and the airborne demonstrator of the future ESA FORUM mission developed by CNR-INO (FIRMOS-B instrument).

https://doi.org/10.5194/essd-2026-557
Preprint. Discussion started: 10 September 2026

2 Instruments

2.1 Airborne demonstrator of ESA FORUM: FIRMOS-B

The Far-Infrared Radiation Mobile Observation System - Balloon (FIRMOS-B) instrument (CNR-INO) has been developed to provide spectrally resolved measurements of the OLR from the stratosphere similar to the measurements that will be delivered by the ESA FORUM sensor, which will cover, for the first time continuously from space, the FIR component. The FORUM space mission has been selected to be the ESA's ninth Earth Explorer mission with an expected launch in 2027. FIRMOS-B is a Fourier transform spectroradiometer (FTS) working in the 100-1600 cm^{-1} spectral range (from 6.25 to 100 µm in wavelength) with 0.4 cm^{-1} of spectral resolution. It uses an interferometric layout with double-input and double-output ports in a Mach-Zehnder configuration. The double-input port setup offers the highest level of radiometric precision and ensures superior spectral quality across the entire spectral range using uncooled detectors. The use of wideband Germanium-coated BoPET (Biaxially Oriented Polyethylene Terephthalate) film beam-splitters together with uncooled pyroelectric DLATGS (deuterated, L-alanine doped triglycine sulfate) detectors, allows achieving a signal-to-noise ratio greater than 300 within 300-700 cm^{-1} spectral interval, with an instrument field-of-view (FOV) of 40 mrad. Three internal black body (BB) sources are employed for accurate radiometric calibration: a reference BB in front of one of the input ports and a calibration unit in front of the measurement input port. The calibration unit consists of a hot BB and a cold BB (both temperatures stabilized) and a folding mirror that enables switching the input between these two reference sources and the radiance from the observed scenario, **Figure 1**. Finally, wavenumber scale calibration is performed using a reference laser system that shares the optical path with the infrared interferometer.

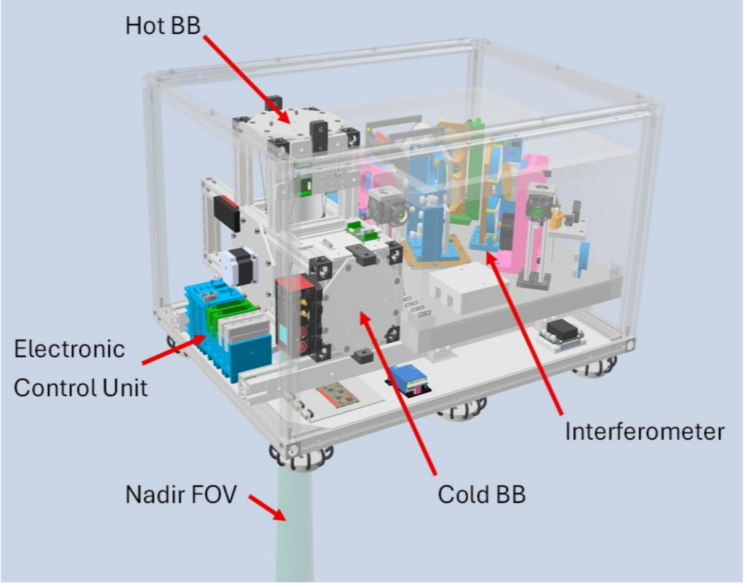

Figure 1. 3D schematic of FIRMOS-B with the main subsystems.

https://doi.org/10.5194/essd-2026-557
Preprint. Discussion started: 10 September 2026

The FIRMOS-B instrument was initially deployed at the Zugspitze observatory for a two-month period of ground-based observations in December 2018 and January 2019 (Palchetti et al., 2021). The results of retrievals of water vapor and cloud properties and their independent validation were published in the Report for Mission Selection for ESA's ninth Earth Explorer (https://esamultimedia.esa.int/docs/EarthObservation/EE9-FORUM-RfMS-ESA-v1.0-FINAL.pdf) and in (Belotti et al., 2023). In August 2022 during the HEMERA-2 campaign, FIRMOS-B underwent its first test on a stratospheric balloon launched from Timmins (Canada) aboard the CNES-CARMEN gondola.

When deployed on a balloon platform, the instrument typically allows observations both in the nadir direction and at the limb, nearly horizontally up to space at +20° above the horizon. During the ATMOSFER 2024 campaign, however, FIRMOS-B was operated exclusively in nadir-viewing mode, acquiring one spectrum every minute with a duty cycle ranging from approximately 50 to 70%, depending on the flight phase, to accommodate regular calibration sequences.

2.2 Pico-Light H_2O

Pico-Light H_2O is the successor of the Pico-SDLA H_2O hygrometer which has been operated since 2007 and allows *in situ* monitoring of atmospheric water vapor in the UTLS. The direct absorption technique allows to unambiguously probe the atmosphere. In such a technique, the laser beam of a 2.63 µm antimonide laser diode is propagated in the open atmosphere over a 1 m distance and is detected with a photodiode. The laser frequency is modulated by ramping the laser current. The absorption spectra are then recorded in situ at over 200 ms. Each atmospheric spectra comprises 1024 datapoints. A period of 800 ms is used to record atmospheric pressure and temperature, GPS data and instrument status. The mixing ratio is retrieved from the atmospheric spectra using a non-linear least square fitting algorithm applied to the full line shape. Pico-Light (weight: 2.7 kg) demonstrates the same performances as the former Pico-SDLA H_2O in-flight. The precision is determined from the standard deviation of the measurements in-flight and is found to be of about 130 ppbv (30 ppbv above the GCOS goal threshold) for a 1s integration time. The hygrometer has been compared to the NOAA FPH instrument during the AsA 2022 (Aire-sur-l'Adour) (Ghysels et al., 2024) and ATMOSFER 2024 campaigns and in chamber during AQUAVIT-4 (Brunamonti et al., 2025). Datasets from Pico-Light are accessible from the HEMERA database (Ghysels et al., 2026).

2.3 The NOAA frost point hygrometer (FPH)

The NOAA FPH (see Fig. 3) is a balloon-borne hygrometer measuring atmospheric water vapor vertical profiles up to altitudes of ~ 28 km. The basic measurement principle and calibration method have remained unchanged since 1980, although the instruments have been significantly modernized over the years (Hall et al., 2016). A thin layer of condensed-phase water (dew or frost) is created and maintained on a highly reflective mirror through rapid feedback temperature control of the mirror. The constant cooling of the mirror is provided by a copper cold finger immersed in trifluoromethane (R23) (or dry ice and alcohol). The air is then flowed at 3–6 $m\,s^{-1}$ through the instrument, at the surface of the chilled mirror. In response to the Kigali Amendment to the Montreal Protocol, NOAA developed the dry ice and alcohol FPH in 2019, which has been compared very well to the NOAA R23 FPH on several occasions and flew during the ATMOSFER campaign in Kiruna in 2024, alongside

https://doi.org/10.5194/essd-2026-557
Preprint. Discussion started: 10 September 2026

Pico-Light and the Cryogenic frost point hygrometer (CFH). A nichrome wire is wrapped around the narrow shaft of the mirror, allowing for an intermittent resistive heating of the mirror. The mirror reflectivity is measured using an infrared LED and photodiode, affected by the amount of condensate on its surface. The frost (dew) point temperature is measured using a calibrated thermistor embedded in the mirror when the condensate layer is stable, indicative of equilibrium between the mirror's condensate layer and the water vapor in the air flowing over it. The partial pressure of water vapor in the flowing air is determined from the frost (dew) point temperature. The water vapor volume mixing ratio is obtained from a division of the partial pressure by the ambient atmospheric pressure, measured by the RS41 radiosonde. Conceptually, frost point hygrometry allows water vapor mixing ratios to be determined from high-accuracy temperature measurements, eliminating the need for water vapor calibration scales or gas standards, which are notoriously difficult to maintain over decadal timescales (Hurst et al., 2011a, 2016). For this campaign R23 was used for the first set of RS flights of the FPH while alcohol and dry ice was used for the second set of RS launches, 08:40 on 27 June. Datasets from NOAA FPH are accessible from the HEMERA database (Hall and Asher, 2026).

2.4 The CFH hygrometer

The CFH measures frostpoints the same way as the NOAA FPH (Vömel et al., 2007). The CFH is one of the few balloon-borne instruments capable of measuring both the tropospheric and stratospheric water vapor mixing ratios with an uncertainty less than 10% for the lowest mixing ratios in the stratosphere (Vömel et al., 2016). Thus, the CFH is very suitable for measuring the especially dry conditions at the tropopause and in the stratosphere up to altitudes of 28km (e.g. (Khordakova et al., 2022)). The CFH typically uses the cooling agent R23 to maintain the cooling of the chilled mirror. We developed a modification for the CFH to use liquid nitrogen (LN2) as the cooling agent in a pressurized vessel. The vessel is kept at a pressure of 200 hPa above ambient to prevent LN2 from freezing below 120 hPa ambient pressures, which would reduce the cooling efficiency of the mirror. Before the campaign, several test balloon launches were flown to adjust the control parameters of the mirror heating to the changed cooling power of liquid nitrogen. The CFHs used during the ATMOSFER campaign still had prototype status. Datasets from CFH are accessible from the HEMERA database (Rolf, 2026).

2.5 LOAC-2 particle counter

LOAC-2 (Light Optical Aerosol Counter - version 2) is a new lightweight optical particle counter developed in 2024 and designed to perform measurements of liquid and solid particles. This instrument is an evolution of the LOAC v1.5 version, which was regularly flown during CNES campaigns, with better sensitivity for the smallest particles, reduced noise and stray light, reduced sensitivity to temperature variations and to electromagnetic interference and increased vertical resolution. The weight of the instrument for a weather balloon flight is 1 kg. The particles are injected into an optical chamber and cross a laser beam; the light scattered is recorded at four scattering angles (compared to only two for LOAC v1.5). The first one is around 15° and is almost insensitive to the refractive index of particles and is used for aerosol counting to retrieve the vertical profiles of the concentrations for 19 size classes between 0.2 and ~50 µm; the other ones are strongly sensitive to the refractive index of particles. By combining measurements at the four angles, it is possible to estimate the typology of the particles (based on their light absorbing properties) when the medium is relatively homogeneous, e.g. minerals, liquid droplets, optically absorbing particles, ice particles.

The number concentration measurements can be converted to extinction, using the equivalent diameter of the particles and their refractive index based on their typology identification. The extinction accuracy is of about 2.10^{-5} km^{-1}. LOAC-2 performs measurements every 10 seconds. With a typical ascent speed of 5 m/s, measurements are available every 50 m. To increase the measurement accuracy in case of low concentration, the data can be averaged over several hundreds of meters; also, the vertical resolution can be adjusted to match those of other instruments. Finally, pressure and temperature measurements are obtained from radiosonde measurements, attached to the instrument.

Although the instrument has substantially evolved in terms of optics, electronics and algorithms, a description of the overall measurement principle (especially at the small scattering angle) can be found in (Renard et al., 2016). The instrument is currently involved in the Atlid/EarthCARE's validation exercise supported by ESA and is expected to be part of the next Strateole2 campaign. Datasets from LOAC v2 are accessible from the HEMERA database (Berthet et al., 2026a).

2.6 The POPS particle counter

The **POPS** (acronym for Portable Optical Particle Spectrometer) is a lightweight (~1 kg) balloon-borne aerosol spectrometer (Gao et al., 2016) manufactured by the Handix Scientific, which is a private company in the USA and used by LPC2E (Laboratoire de Physico-Chimie de l'Atmosphère) since 2018. The instrument is adapted to fly with latex weather balloons from different sites around the world (e.g. (Asher et al., 2024; Kloss et al., 2020; Todt et al., 2023)). It uses a 405-nm laser diode. Ambient air is drawn through an 1/8-inch inlet nozzle to the optical chamber with a controlled flow of 3.5 cc s^{-1} at the surface (the flow rate is increased in the stratosphere). The laser beam is focused using a cylindrical lens to maximize the signal-to-noise ratio and the uniformity of the vertical laser intensity. The amount of detected elastically scattered light is determined from the measured electrical current from a photomultiplier. POPS delivers aerosol number concentration and size distribution measurements in the range 0.140–3 µm diameter. Reaching particle sizes below 0.2 µm diameter is possible owing to the blue diode. Mismatches between refractive indices used for instrumental calibration and atmospheric particles are identified as primary source of measurement error (Asher et al., 2024). However, this effect is dramatically reduced for sulfuric acid droplets, which are abundant in the stratosphere. POPS achieves a vertical resolution of approximately 100 m, with a time sampling of 1 second. This combination allows for high-resolution temporal and spatial profiling of aerosols. Datasets from POPS are accessible from the HEMERA database (Berthet et al., 2026b).

2.7 The NIXE-B instrument

NIXE-B is a balloon-borne instrument suite that measures ice particles in two complementary size ranges. Particles larger than 20 µm diameter are analyzed with an imaging module. Ice crystals are collected on an oil-coated film, transported beneath a microscope and photographed with a high-resolution camera (Kuhn and Heymsfield, 2016). The high-definition images are

https://doi.org/10.5194/essd-2026-557
Preprint. Discussion started: 10 September 2026

stored on an onboard computer and evaluated post-flight, yielding information on cloud particle size, shape, and number. Smaller particles between 0.4 and 40 µm diameter are characterized with an OPC-N3 instrument modified at the University of Hertfordshire and dubbed the UCASS-N3 (Smith et al., 2019), which records light-scattering data and derives particle-size distributions in real time. The modification allows the instrument to be naturally aspirated, rather than sampling with a fan, thereby reducing sampling issues related to altitude and relative windspeed. By combining these two techniques, NIXE-B spans the entire spectrum of cirrus-cloud ice particles. The instrument was deployed during the ATMOSFER-2024 campaign, flying both on the ATMOSFER gondola and on a free-release balloon accompanying the zero-pressure balloon (ZPB). Datasets from NIXE-B are accessible from the HEMERA database (Afchine, 2026).

2.8 The Laser Particle Counter (LPC)

The LASP particle counter (LPC) is a modification of the LASP optical particle counter (LOPC). Both instruments use dark field microscopy to measure side scattered light from particles passing through the sensing region. The light scattered is from a 780 nm diode laser and the collection optics are oriented at 90° from the optical path with a collection angle of 3.6 steradians. The LPC measures the concentration of particles > 0.3 – 24 µm diameter with 32 size bins. The size range for the LOPC is the same but relays the data in 50 size bins. The LOPC has been described by (Kalnajs and Deshler, 2022), is flown routinely for stratospheric aerosol measurements from Boulder, Colorado (Deshler and Kalnajs, 2026), and has been used for sounding measurements from McMurdo Station, Antarctica (Deshler et al., 2024). The optics and particle sensing electronics of the LPC and LOPC are identical. The instrument is characterized by a counter response function derived from the instrument characteristics and Mie scattering theory to relate the electronic pulses to the particle size (Kalnajs and Deshler, 2022). For stratospheric aerosol solution droplets Mie scattering is a good assumption, but does require knowledge of the particle index of refraction. The differences between the LPC and LOPC are in data transmission and storage, and interfaces to a radiosonde typically flown with the LOPC. For the LPC there is no instrument attached for state parameters and the data are transmitted to the Strateole2 Zephyr data control center, which is then responsible for transmitting data packets through the Iridium network to the surface receiving station. In this configuration the LPC has a measurement frequency of 0.5 Hz at a cadence of 3 minutes of measurements every 30 minutes. For ATMOSFER this cadence was at times reduced to 3 minutes for every 10 minutes. Datasets from LPC are accessible from the HEMERA database (Deshler and Kalnajs, 2026a).

3 The flights

The FIRMOS-B instrument was flown onboard the CARMENCITA gondola of CNES, together with the POPS, LOAC v1.5 and NIXE-B particle counters and imager. The gondola included 12 different instruments, 4 of which were dedicated to the FORUM preparatory activities, and which constituted the ATMOSFER gondola (see **Fig. 2**). The LPC instrument was flown as part of the Strateole2 Zephyr gondola onboard the same Zero Pressure Balloon (ZPB).

https://doi.org/10.5194/essd-2026-557
Preprint. Discussion started: 10 September 2026

Open Access Earth System Science Data Discussions

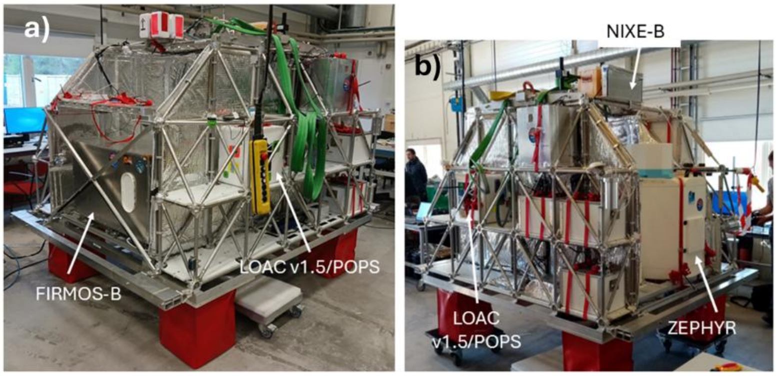

Figure 2: Pictures of the ATMOSFER gondola carrying FIRMOS-B (panel a), NIXE-B, POPS and LOAC v1.5 instruments (panel b).

The ZPB ATMOSFER was released at 23:02 UTC from the Esrange Space Center in Kiruna, Sweden (67°N) on June 26, 2024. The flight lasted 11 hours with a first float near 32 km, which lasted 2 hours, followed by a second float near 20 km which lasted 4.5 hours, before a slow descent at 5 m s^{-1} and a termination at 10:00 UTC (see flight profile on **Fig.3**). Aside from the ZPB ATMOSFER, six small weather balloons (RS balloons) were released during the ascent and early descent of the ZPB. Three RS balloons were released within 40 minutes after the release (at 23:40 UTC on June 26, 2024, RS group 1) of the ZPB ATMOSFER and three others were released at 08:40 UTC on June 27, 2024, less than an hour before the final descent of the ZPB ATMOSFER (RS group 2). Each RS balloon carried a single hygrometer: Pico-Light H_2O, NOAA FPH or CFH to limit contamination of the measurements from outgassing. The NOAA FPH hygrometer was flown together with an ECC ozonesonde. The flight chains of each RS flight are given in **Fig. 4**.

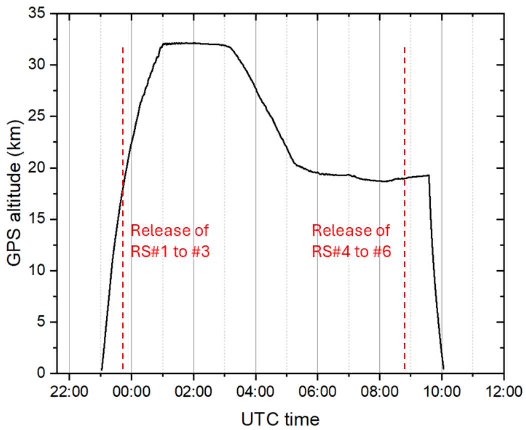

Figure 3: Flight profile of the ZPB ATMOSFER during the CNES campaign from l'Esrange Space Center (Kiruna, Sweden) on June 26, 2024 (black line). The time for the release of the RS flights is indicated with dashed red lines.

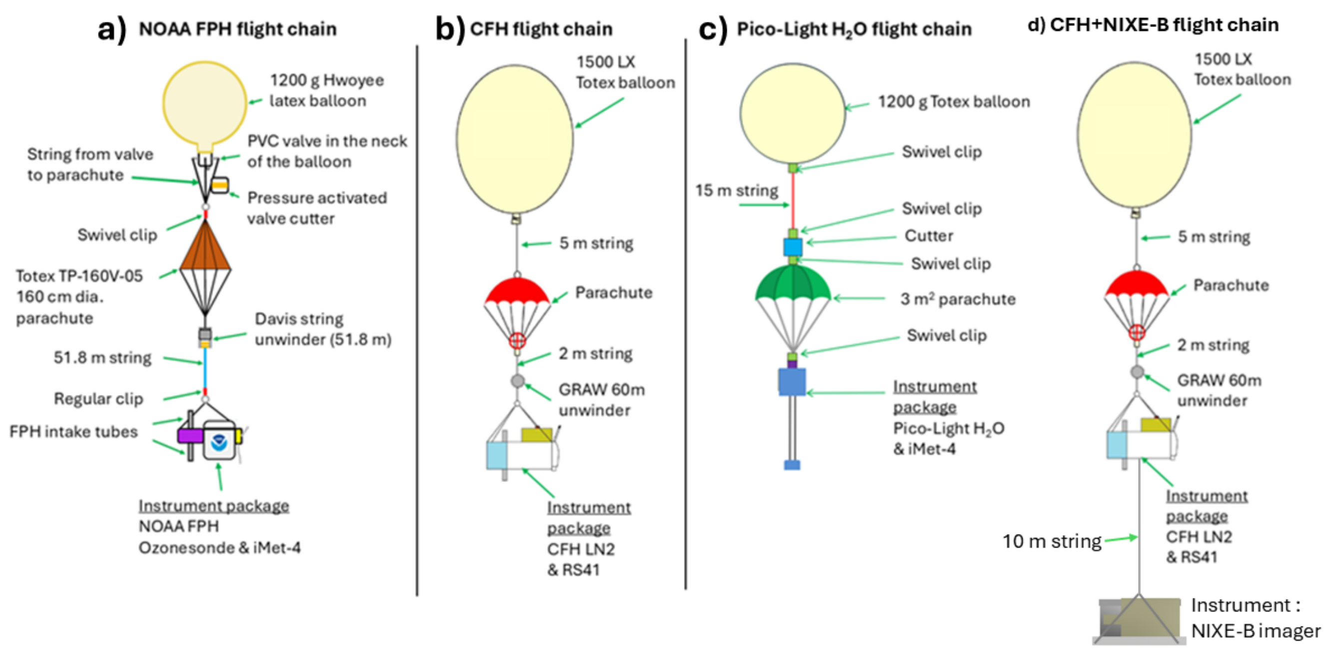

Figure 4: Flight chains of the RS flights during the ATMOSFER campaign, on June 26, 2024, from Esrange Space Center (Kiruna, Sweden). Panel a) Flight chain of NOAA FPH, panel b) flight chain of CFH, panel c) flight chain of Pico-Light H_2O and panel d) flight chain of CFH including NIXE-B.

For both NOAA FPH and CFH flight chains, the distance between the hygrometers and the parachute and balloon is at least 50 m. In the case of Pico-Light H_2O, the parachute is directly attached to the top of the instrument using a swivel clip. The distance between the parachute and the balloon is then 15 m.

During the second session of RS launches (at about 08:40 UTC), the CFH flight chain included the NIXE-B instrument (see panel d, on **Fig. 4**), located downstream of the CFH by 10 m.

4 Data quality assessment

The far infrared (FIR) radiances are sensitive to water vapor in the UTLS and to thin cirrus clouds. Several hygrometers have been launched a few minutes apart, offering the possibility for quality assessment of water vapor data. For further studies, water vapor datasets will be useful for activities around the evaluation of FIRMOS-B (and subsequently FORUM) including an evaluation of UTLS water vapor, cloud-top and atmospheric state retrieval accuracy in clear-sky and cloudy conditions. For aerosols and ice particles, the participating instruments provide complementary observations. LOAC-2 appears particularly adapted for the characterization of different particle types (concentrations for 19 size classes between 0.2 and ~50 µm) whereas POPS's observations are particularly relevant for small liquid droplet sizes (0.140–3 µm) and fine vertical structures of the aerosol content. Both instruments can properly capture volcanic and smoke plumes in the stratosphere. The NIXE-B instrument

https://doi.org/10.5194/essd-2026-557
Preprint. Discussion started: 10 September 2026

measures ice particles in two complementary size ranges: particles larger than 20 µm are analyzed with an imaging module while particles between 0.4 and 40 µm are characterized with a modified OPC-N3 instrument. NIXE-B can then span the entire spectrum of cirrus-cloud ice particles. It is however possible to perform cross validation since the package of particle instruments permits overlapping of size distribution data.

4.1 Water vapor

4.1.1 Outgassing contamination

Measuring water vapor, especially in the UTLS and stratosphere, remains highly challenging. Typical mixing ratios of water vapor in the UTLS are below 10 ppmv. Substantial discrepancies between different airborne measurement techniques can still be observed due to measurement contamination originating from outgassing of water vapor molecules from any instrumental and flight chain surfaces. Significant improvements have been made on instrument sampling strategy, building materials and flight chain configurations over the last decades to mitigate these issues. The hygrometers flown during the ATMOSFER campaign are among the few instruments capable of providing reliable measurements of water vapor in the UTLS. Each instrument developed its specific strategy to limit outgassing contamination:

- The optical cell of Pico-Light H_2O is open to the atmosphere, made of carbon fiber with limited surface on which adsorption might take place. Additionally, the instrument probes the UTLS mainly during the descent, after the balloon burst, to suppress the contamination from the balloon wake.
- The NOAA FPH and CFH hygrometers sample ambient air through a clean 18 cm long stainless-steel tube, designed to eliminate contamination from instrument outgassed water vapor.
- Finally, both NOAA FPH and CFH are flown hanging on hydrophobic tethers below the flight chain at a distance larger than 40m, as specified by the World Meteorological Organization (WMO) (Immler et al., 2010) to reduce the impact of outgassing from the balloon and parachute.

Due to the short CNES flight chain of Pico-Light H_2O, the water vapor data of the instrument are of scientific value during the descent and during the ascent in the troposphere (below the lapse rate tropopause). The lapse rate tropopause altitude for each of the 2 sessions of RS launches (23:40 UTC and 08:40 UTC) varies from 10.5 and 11.5 km respectively. Future flights of the hygrometer by CNES will be performed under a 40-m hydrophobic tether, following the WMO recommendations.

4.1.2 Saturated layers: clouds

4.1.2.1 RS group 1

The hygrometers flew through a thick ice saturated cloud during the ascent of the first session of small balloon launches. The saturation mixing ratio over ice is calculated from the *in-situ* hygrometers' measurements, using the Goff Gratch (1984) saturation vapor pressure over ice equation.

https://doi.org/10.5194/essd-2026-557
Preprint. Discussion started: 10 September 2026

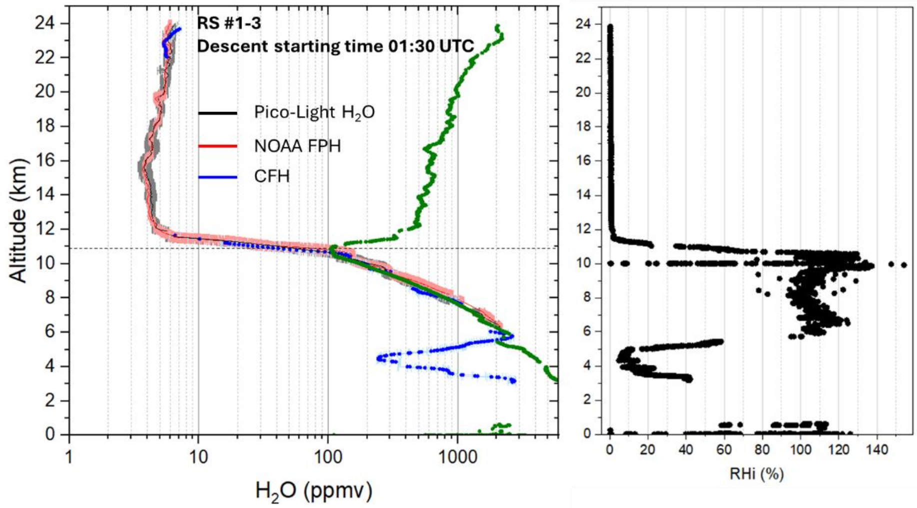

Figure 5: Left panel: Comparison of water vapor vertical profiles from Pico-Light H_2O (black line), NOAA frost point (FPH, red line) and Cryogenic frost point hygrometer (CFH, blue line) during the first session of sounding balloon launches of the ATMOSFER campaign (June 2024) from the Esrange Space Center (Kiruna, Sweden). The ice saturation mixing ratio (green line) has been calculated from Pico-Light H_2O water vapor and temperature measurements, using the Goff Gratch (1984) saturation vapor pressure over ice equation. Right panel: Vertical profile of RHi calculated from Pico-Light H_2O measurements. High ice saturation if found between 6 and 11 km.

Figure 5 shows the comparison of water vapor measurements during the descent of Pico-Light H_2O, NOAA FPH and CFH as well as RHi from pico-Light H_2O measurements. The ice saturation mixing ratio is displayed to identify the layers of saturation where clouds were present. All three hygrometers show the thick ice saturated layer expanding from 6 to about 11 km, with RHi ranging from 80 to 130%. The presence of a thick ice cirrus cloud is confirmed by the ice imager of NIXE-B which shows large ice crystals of size around 270 µm, near 8.4 km, as well as by the ice crystal size distributions of NIXE-B (see section 4.3.1) and visible images taken by FIRMOS-B onboard the ATMOSFER ZPB.

Following the ascent through this saturated cloud layer, the measurements of the CFH instrument were contaminated from the lapse rate tropopause (here at 10.5 km) up to 18.3 km. Subsequently, CFH data in this altitude range are not suitable for scientific analysis.

The NOAA flight train includes a valve (e.g., Fig. 4) (Krauchi et al., 2016) that allows for descent as well as ascent data to be collected at the same rate in the stratosphere; valved balloons can then travel long distances, and data telemetry of the full descent is often not available.

https://doi.org/10.5194/essd-2026-557
Preprint. Discussion started: 10 September 2026

4.1.2.2 RS group 2

During the ascent of this second session of launches, a thin layer of ice saturation is observed at the tropopause (11.1 – 11.6 km) by Pico-Light H_2O, by NOAA FPH (10.8 – 11.8km) and CFH (10.2 – 11.8 km). A thick layer of high RHi (80<RHi<100%) is observed between 3.9 and 7.8 km, with variability between instruments.

During the descent of session#2, two layers of ice saturation are observed by Pico-Light H_2O, one between 10.4 and 10.8 km and the other between 11.3 and 11.6 km. In the first case, RHi as high as 115% are observed while in the second case, the RHi values are around 102%. These two layers are separated by a layer of RHi~80% (altitude range: 10.7 – 11.3 km). During the descent, the Pico-Light H_2O instrument falls under a parachute, which leads to a landing 95 km away from the launching point. In the case of NOAA FPH, the landing occurred 195 km away. Ice saturated layers are also observed by NOAA FPH, at slightly different altitudes, between 10 and 10.9 and between 10.9 and 11.8 km. Unfortunately, no aerosol measurements were performed during this session.

4.1.3 Inter-instrumental comparisons for water vapor

Within each of the two sessions, the hygrometers were released a few minutes apart to facilitate cross-comparisons between each hygrometer. Water vapor mixing ratios from the hygrometers are averaged over 150 m bins before comparisons between instruments are performed. The tables 1, 2 and 3 list the relative differences in water vapor mixing ratios between pairs of hygrometers. The troposphere is defined as the altitude range between ground and the lapse rate tropopause altitude, and the stratosphere at altitude higher than the lapse rate tropopause altitude.

We limit the comparisons to the ascent for the troposphere to limit as much as possible a degradation of the comparison due to high tropospheric water vapor variability in the context where each hygrometer flew under its own balloon. We select tropospheric data from ground up to the altitude of the lapse rate tropopause for ascent datasets. The stratospheric comparisons are limited to descent data, for which the Pico-Light H_2O instrument could provide reliable measurements. Data are considered for altitude from the lapse rate tropopause up to 24.5 km. Measurements from FPH are used as reference. The data from Pico-Light, CFH and FPH data are averaged over bins with an altitude of ± 100 m prior to calculate the relative difference which is defined as:

$$x_k = \left(\frac{\chi_{pico/CFH} - \chi_{FPH}}{\chi_{FPH}}\right) x\ 100 \quad (1)$$

where $\chi_{pico/CFH}$ and χ_{FPH} are the average mole fractions from Pico-Light or CFH and FPH over the ± 100 m altitude bins. The mean relative differences listed in table 1 is the mean of each x_k over the whole altitude range considered.

The weighted average is calculated such as:

$$\bar{x} = \sum_{k=1}^{N} \frac{\bar{x}_k . n_k}{n_k} \quad (2)$$

where $\bar{x}$ is the weighted average of means, k is the number of each data group, n is size of the dataset in group k and N the total number of groups. The weighted standard deviation ($\bar{\sigma}$) is calculated such as:

https://doi.org/10.5194/essd-2026-557
Preprint. Discussion started: 10 September 2026

$$\bar{\sigma} = \sum_{k=1}^{N} \frac{\sqrt{(n_k-1).\sigma_k{}^2}}{n_k-N} \quad (3)$$

where σ_k is the standard deviation for a given group of data.

4.1.3.1 Comparison between Pico-Light H_2O and NOAA FPH

ATMOSFER 2024	FPH	Pico-Light	Alt range (km)	Session #1 (R23 FPH) (23:40UTC)	Session #2 (dry ice/alcohol FPH) (08:40 UTC)	Weighted average
Troposphere	Ascent	Ascent	0.9-10.5 (session #1) 0.4-11.5 (session #2)	-6.3 ± 14.1 %	3 ± 14 %	-1.5 ± 14.0 %
Stratosphere	Descent	Descent	10.5-24.5 (session #1) 11.5-24.5 (session #2)	0.8 ± 7.1 %	10 ± 10.4 %	4 ± 8.4 %

Table 1: Comparison between water vapor mixing ratio retrievals from Pico-Light H_2O and NOAA FPH during the ATMOSFER 2024 campaign from Kiruna (June 2024). The percent differences are calculated using FPH as the reference using Eq. 1 and the standard deviations are calculated following Eq. 3.

Results from the comparison show a good agreement between Pico-Light H_2O and NOAA FPH, both in the troposphere and in the stratosphere, especially for session#1 where the R23 version of FPH was flown. The differences for session#1 are better than 1% on average in the stratosphere. The standard deviation is of ~7%, larger than previous comparisons between Pico-Light H_2O and FPH (~4.6% (Ghysels et al., 2024)). This is mainly attributed to a sharp vertical gradient of water vapor (72 ppmv/km) within 1 km around the tropopause altitude which challenges the dynamical range of FPH instrument. If we exclude this 1 km transition layer (altitude range for comparison : 12 – 24.5 km), the comparison improves for the session #1 stratospheric comparison with a mean difference of 2.6 ± 2.9%, in line with previous published comparison during the AsA 2022 campaign when the R23 version of FPH was flown (Ghysels et al., 2024) (stratospheric differences : 2.4 ± 4.6%).

Larger differences are observed in the stratosphere when comparing Pico-Light H_2O and the dry ice and alcohol version of NOAA FPH. Differences are of 10 ±10.4 %, with largest differences observed just above the lapse rate tropopause altitude (altitude range: 11.5 – 16.0 km). Again, a sharp vertical gradient of water vapor (100 ppmv/km) has been observed within 1km of the lapse rate tropopause altitude (altitude range: 11.6 – 12.4 km), which could have produced instabilities in the control loop of FPH. The addition of PID software controls have since sought to improve such potential problems. Excluding this portion of the profile for comparison and considering only altitudes above 16 km, leads again to results in line with the AsA 2022 results, with differences of 2.9 ± 4.7 %, demonstrating the measurement reproducibility of both instruments.

In the troposphere, the comparison is also excellent with differences of -6.3 to + 3%, and a variability of ~14%. During AsA 2022, the mean relative difference between Pico-Light H_2O and FPH was of 3.8 ± 23.6 %, while in this case it is of -1 ± 17 %. The high natural variability of tropospheric water vapor limits the inter-instrument agreements to a few percents, while the less variable stratosphere permits more reliable comparisons and allows evaluations of instrumental reproducibility.

https://doi.org/10.5194/essd-2026-557
Preprint. Discussion started: 10 September 2026

Open Access Earth System Science Data Discussions

4.1.3.2 Comparison between Pico-Light H_2O and CFH

ATMOSFER 2024	CFH	Pico-Light	Alt range (km)	Session #1	Session #2	Weighted average
Troposphere	Ascent	Ascent	0.9-10.5 (session #1) 0.4-11.5 (session #2)	-4 ± 14 %	-5 ± 11 %	-5 ± 12 %
Stratosphere	Descent	Descent	10.5-24.5 (session #1) 11.5-24.5 (session #2)	12 ± 18 %	-16.5 ± 14.6 %	-14.8 ± 14.8 %

Table 2: Comparison between water vapor retrievals from Pico-Light H_2O and CFH during the ATMOSFER 2024 campaign from Kiruna (June 2024).

Results from the comparison show a good agreement in the troposphere, with mean difference of about -5 ± 12 %. During both sessions of flight, the LN2 version of CFH was released, which was a new version of the instrument in test status.

All three instruments have sampled a thick ice saturated airmass, in the altitude range from 6.0 to 10.5 km (see **figure 6**). Measurements from CFH above 10.5 km are probably contaminated by the evaporation of ice crystals trapped in the intake tube of CFH following the flight across this thick layer.

Stratospheric comparisons are made using descent profiles of all instruments. The comparisons show much larger differences (~ 15%) for CFH compared to results of comparison with FPH. For both sessions, since CFH was operated under regular free-release balloon (no valve), oscillations in the stratospheric profiles of the CFH results probably from the difficulty to reach thermal dynamic equilibrium due to a very fast stratospheric descent rate of 60 m s^{-1}.

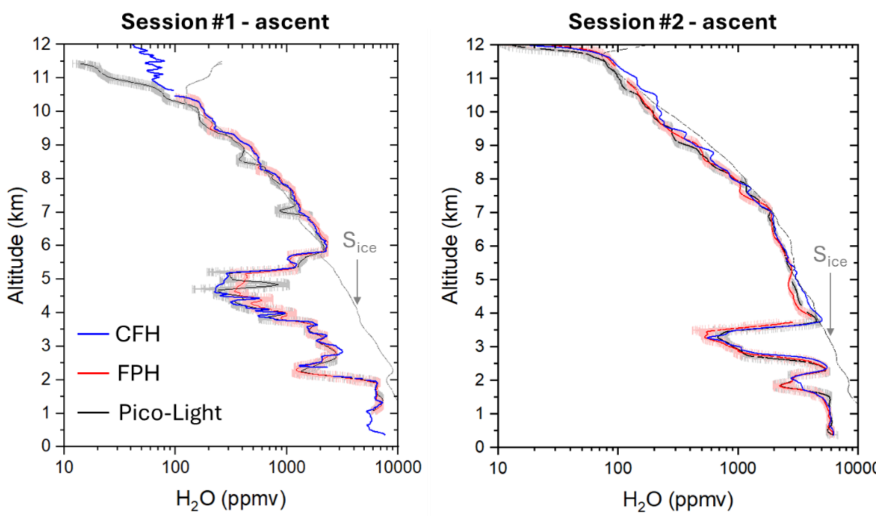

Figure 6: Vertical profiles of water vapor during the ascent of session #1 and 2 of all three hygrometers (Pico-Light, FPH and CFH) from Kiruna, Sweden in June 26-27, 2024. The thin grey line indicates the saturation mixing ratio over ice, indicating layers of ice saturation.

4.1.3.3 Comparison between NOAA FPH and CFH

ATMOSFER 2024	FPH	CFH	Alt range (km)	Session #1	Session #2	Weighted average

https://doi.org/10.5194/essd-2026-557
Preprint. Discussion started: 10 September 2026

Troposphere	Ascent	Ascent	0.9-10.5	-4.2 ± 12.2 %	12.2 ± 14.6 %	4.3 ± 13.5 %
Stratosphere	Descen t	Descen t	10.5-30.2 10.5-24.5	-8.9 ± 18.1 % -8.9 ± 18.1 %	37.3 ± 24.9 % 37.1 ± 19.8 %	24.6 ± 23.2 % 23.1 ± 19.3 %

Table 3: Comparison between water vapor retrievals from NOAA FPH and CFH during the ATMOSFER 2024 campaign from Kiruna (June 2024).

The differences in the troposphere scale from -4 to 12 % on average for session #1 and 2 respectively, with a weighted average around 4.3 % including both sessions. Again, the largest differences are observed for session #2 with a mean difference of around 12 % where a newly developed prototype of CFH from En-Sci was flown. Stratospheric comparisons (descent measurements) are restricted to the range 22 to 24 km for session #1 where smaller differences have been observed, while larger differences (~37 %) are observed for session #2. These disparities can be explained by poor functioning of the CFH instrument stabilization controller which had issues to stabilize the mirror temperature. Such an issue has been reoccurring in the testing of the LN2 version of the instrument.

4.2 Ozone: dynamic tracer

Ozone sondes were flown with each NOAA FPH, allowing for tracing of airmass origin. The dataset includes ozone vertical profiles provided by En-sci ECC 2Z ozone sondes from ground up to 30 km for both sessions of RS balloon launches. The accuracy of ozone retrievals is given at ± 5% between 1000 and 4 hPa and the effective vertical resolution is of approximately 150 m. Figure 7 shows vertical profiles of water vapor from the descent of Pico-Light and NOAA FPH and of ozone from the ECC sonde attached to the NOAA FPH instrument during ATMOSFER flights.

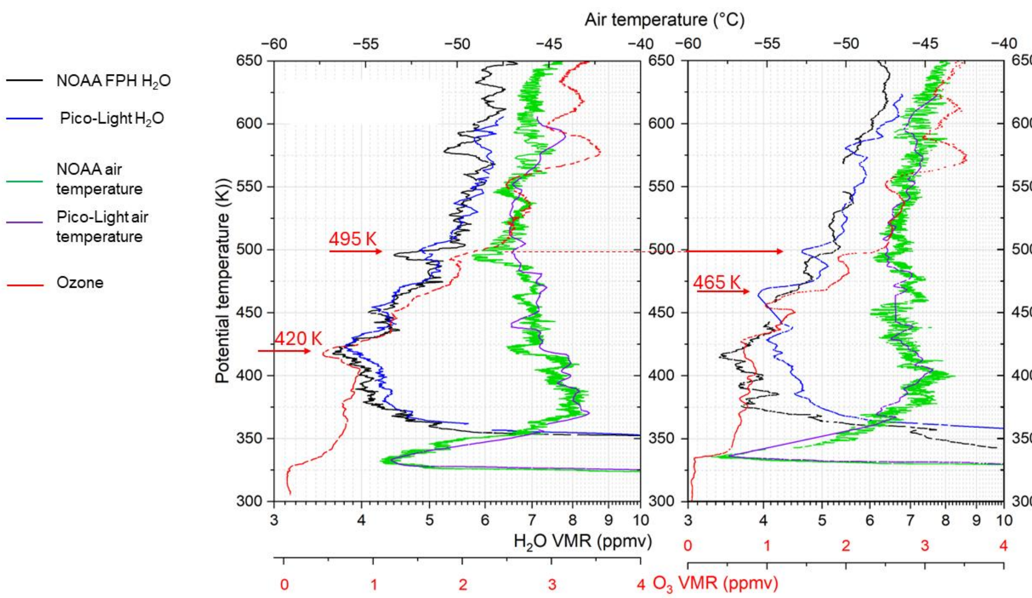

https://doi.org/10.5194/essd-2026-557
Preprint. Discussion started: 10 September 2026

Figure 7: Descent vertical profiles of water vapor, temperature and ozone during the first (left) and second (right) session of RS balloon launches of the ATMOSFER campaign from Kiruna, Sweden in June 2024. Black profiles are NOAA FPH profiles, blue profiles are Pico-Light H_2O profiles of water vapor. Red profiles are ozone profiles from the ECC sonde flown in tandem with NOAA FPH. Air temperature profiles are given for Pico-Light (purple line) and NOAA FPH (green line). The red arrows mark the position of layers of interest.

Both sessions of launches have been released 9 hours apart. Yet, differences are observed between 10 and 20 km (327 K and 511 K isentropic levels) in the vertical structures of ozone and water vapor, suggesting different airmasses. Dry layers, low ozone, are observed on three altitude levels on the profiles of both sessions: near the isentropes 420 K (~15.5 km), 465 K (~18 km), 495 K (~ 19.6 km).

To trace the origin of the airmasses, simulations using the MIMOSA model (Modélisation Isentrope du transport Méso-échelle de l'Ozone Stratosphérique par Advection) (Hauchecorne et al., 2002) have been performed on the 420, 465 and 495 K isentropic levels. **Figure 8** shows potential vorticity maps on the selected isentropic levels. On these maps we plot the modified potential vorticity (Lait, 1994), which is defined as $Lait_{PV} = PV\left(\frac{475}{\theta}\right)^{9/2}$ where PV is the Ertel's potential vorticity, θ is the isentropic level (in K). The potential vorticity is used as a diagnostic of dynamical processes in the stratosphere.

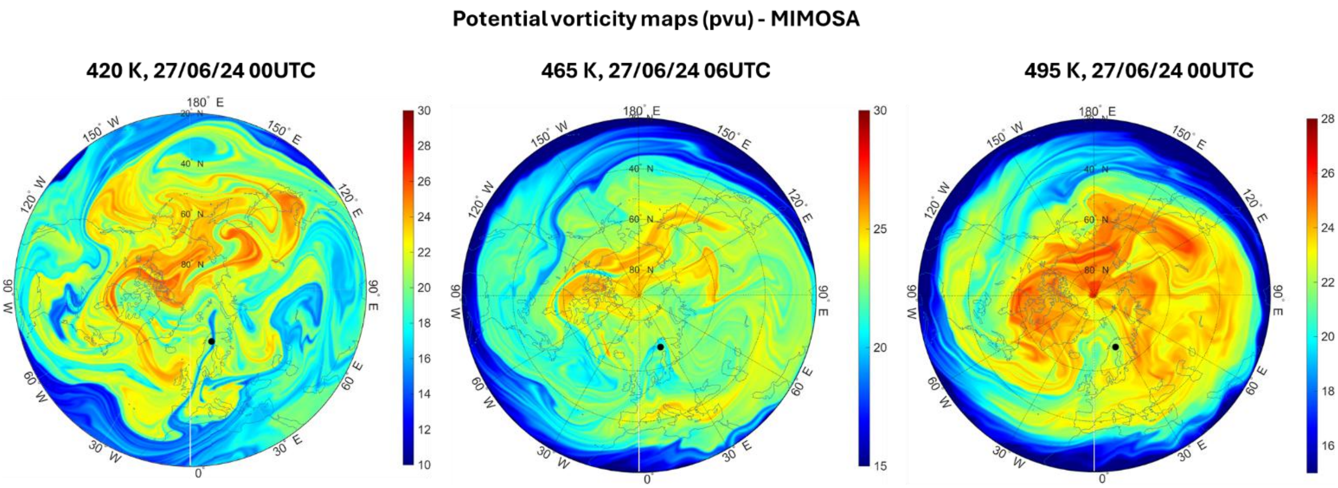

Figure 8: Potential vorticity maps from the MIMOSA model on the isentropic levels 420 K (left), 465 K (center) and 495 K (right) for June 27, 2024 at 00 and 06 UTC. The balloon position is marked with a black dot.

The analysis using potential vorticity shows that the dry low ozone layer near 15.5 km (420 K), corresponds with the intrusion of a tropical filament at high latitudes while the two other structures near 18 and 19.6 km correspond to airmasses at mid-latitudes.

https://doi.org/10.5194/essd-2026-557
Preprint. Discussion started: 10 September 2026

Open Access Earth System Science Data Discussions

4.3 Particles

A complementary set of optical particle counters and an imager have been released under RS balloons and onboard the ZPB ATMOSFER to capture the size distribution, number concentrations of aerosols and ice particles. A variety of signatures have been observed during the flights: cirrus clouds, volcanic plume and fire plumes, which are described hereafter and which are essential for the accurate retrievals of radiance measurements from FIRMOS-B.

4.3.1 Cirrus cloud between 6 and 10 km

As seen in section 4.1.2, during the ascent of the ZPB ATMOSFER and of session #1, a thick layer of ice saturation has been observed between 5.8 and 9.7 km from the hygrometers under RS balloons. Simultaneous observations of aerosols have been performed from POPS, LOAC v1.5, NIXE-B and LPC onboard the ZPB which are shown in **figure 9**. Small particles are found in 4 layers between 2.8 and 9.2 km (see POPS profile in the center), with diameters consistent between all instruments, below 1µm. The intermittent data from the LPC is by design, since this was an engineering flight for future deployment of the LPC on long duration balloons with intermittent sampling.
The figure also shows large particles observed by both LOAC v1.5 (diameter ranging from 3 to 8 µm) and NIXE-B N3-OPC (diameter from 3 to 8 µm) near 6.8 km, at the top of the first three layers of small aerosols which extend vertically from 2.5 to 6.8 km. The altitude at which the large aerosols are found corresponds to a depleted layer of small aerosols.

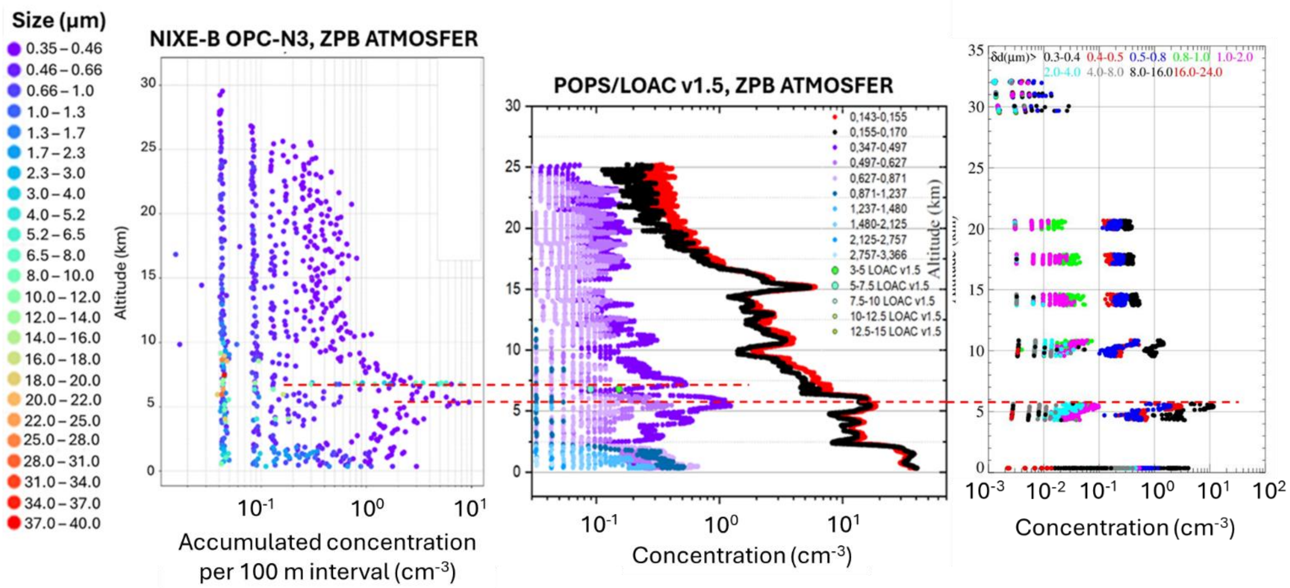

Figure 9: Particle size distributions from NIXE N3 OPC (left panel), POPS and LOAC v1.5 (center panel) and LPC (right panel) from ground up to 30 km of altitude onboard the ZPB ATMOSFER. The red dashed lines show layers where peaks of size particle concentrations are found, and where large particles were detected by both LOAC v1.5 and NIXE OPC.

https://doi.org/10.5194/essd-2026-557
Preprint. Discussion started: 10 September 2026

Open Access Earth System Science Data Discussions

Between 8 and 8.5 km, the NIXE-B instrument both onboard the ZPB ATMOSFER and RS balloon (session#1 ascent) observed ice crystals distributed within 5 groups: compact, plate, irregular, column and rosette (see Fig. 10). The analysis of NIXE-B imager's measurements provided a percentage shape distribution of crystals. Ice crystals have been observed by both NIXE-B instruments under RS balloon and onboard the ZPB, with similar vertical distribution. The figure 10 provides also ice crystal shape distribution and area equivalent diameter for the ascent of the ZPB ATMOSFER and the RS balloon flights. The equivalent area diameter for both flights show large crystals with area equivalent diameter scaling from 50 to 400 µm. During session#1, one of the RS balloons was carrying the CFH hygrometer and the NIXE-B instrument. In the case of this flight, we can observe that the larger crystals (area equivalent diameter >200 µm) are found around 8.5 km, where RHi (calculated from CFH collocated measurements) is depleted from 120% down to 90%. Large dispersion in crystal equivalent diameter is found in the range where a sequence of ice saturated and non-saturated layers is found (i.e. between 6 and 9 km).

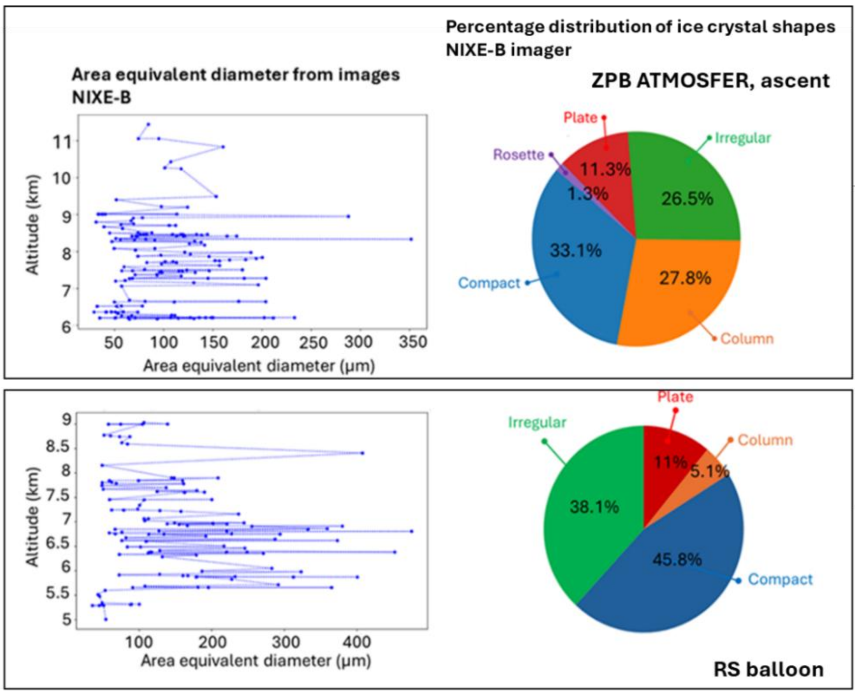

Figure 10: Area equivalent diameter and ice crystal shapes from the NIXE-B instrument both onboard the ZPB ATMOSFER and under RS balloon (session#1) during the ATMOSFER campaign from Kiruna, Sweden, in June 2024 (left and center).

The large crystals are found at air temperatures between 235 and 240 K.

The cirrus observation is further confirmed by satellite Sentinel 5P (S5P) observations such as illustrated in **Fig. 11**. In this case, the coincidence between SP5 overpass and balloon position confirms strongly the presence of cirrus near 9 km. The RS balloons of session #1 reached altitudes near 9km between 00:10 and 00:40 UTC on June 27, 2024. The top cirrus altitude deduced from in situ aerosol observations is located near 9.4 km, with a saturated layer extending to 10.1 km. These are close to S5P retrieved top estimations between 8.4 and 9.1 km.

https://doi.org/10.5194/essd-2026-557
Preprint. Discussion started: 10 September 2026

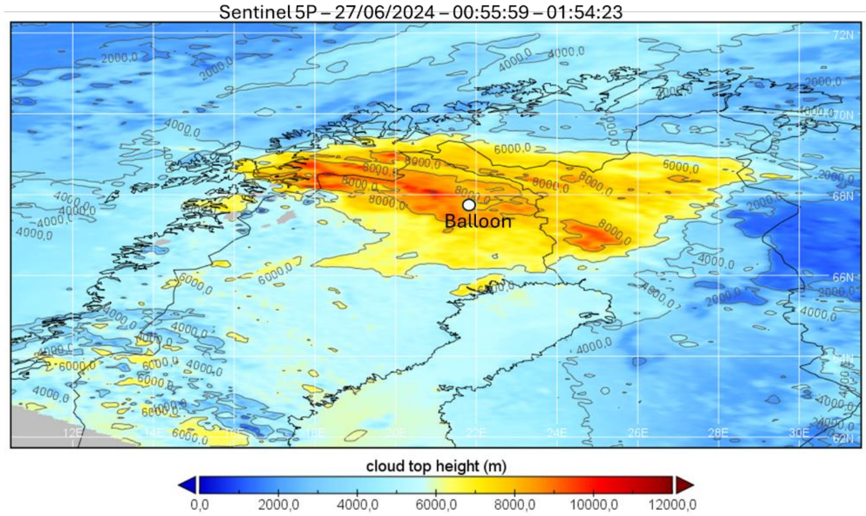

Figure 11: Cloud top height map from Sentinel 5P observations, for June 27, 2024 early morning, above Sweden. The balloon position near 9km, within 1h of SP5 overpass, is indicated with a white filled circle.

Analysis using the MIMOSA model suggests that this layer originates from a filamentary structure originating from the edges of high PV airmasses, which stretches up to Canada. This is confirmed by ensemble isentropic back-trajectory analysis using the HYSPLIT model for altitudes between 8 and 10 km. The model has been initiated using global meteorological data from GFS (resolution: 0.25°) from the location of the balloon carrying NIXE-B (RS session #1 and ZPB balloon, Fig. 10) near the altitude of detection of the large crystals and collocated low aerosol layer from POPS/LOAC (8.1 and 9.6 km altitude, latitude:67.91°N; longitude: 21.67°E).

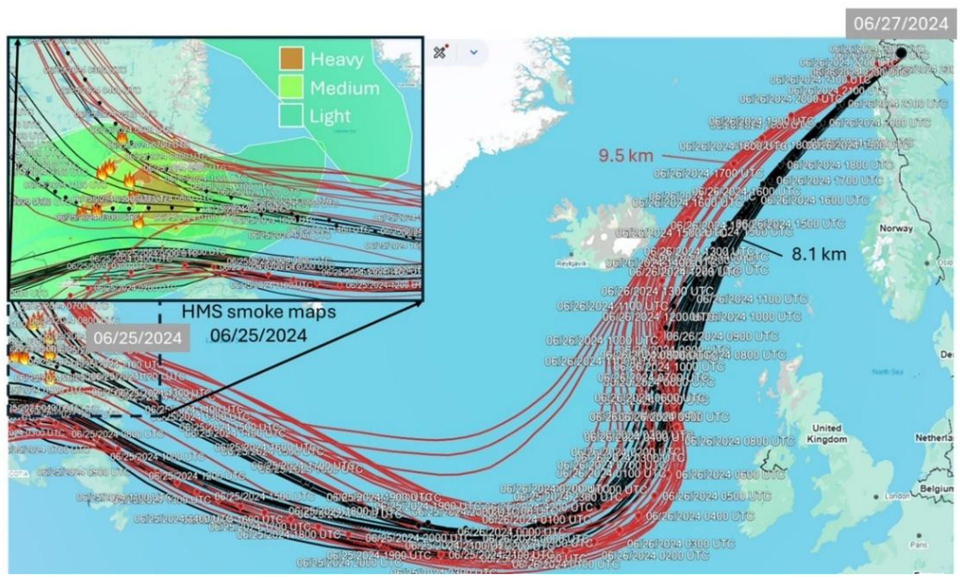

Figure 12: Ensemble back trajectories calculated using the HYSPLIT model, at altitudes of 8.1 and 9.5 km, from the location of the observed cirrus and aerosol plumes sampled by the different optical particle counters onboard the ATMOSFER ZPB gondola and free-release balloons.

https://doi.org/10.5194/essd-2026-557
Preprint. Discussion started: 10 September 2026

The NOAA Hazard Mapping System (HMS) fire and smoke products show several fires over Labrador and Quebec in Canada and North East of the US on June 24, 2024, which are overpassed by the airmasses sampled during the flight between June 24 and June 25, 2024. The area overpassed by the airmasses on June 25 have been classified as heavy smoke areas by HMS (see **Fig. 12**). On top, several fire events occurring during the period from May 9 to June 25, 2024, mainly over British Columbia with a large event on May 9. SAGE III and ACE-FTS extinction ratio profiles at 521 and 1020 nm show the presence of a strong plume between 10 and 12 km following the event which persist over the following several weeks and reach higher latitudes within the few days following the event. Therefore, a combination of fire events spreading over the period from May 9 to June 25 could be the origin of the observed aerosol plume below the tropopause.

Hygrometers data allowed to calculate the relative humidity over ice (RHi) along the balloon trajectory during the ascent of session #1. Saturation inside the thick layer between 6 and 10 km varies from 100 to 137% for air temperature varying between 220 and 253 K. This level of saturation excludes homogeneous freezing. Ice water content (IWC) has been calculated from NIXE-B datasets aboard the free-release balloon, jointly with CFH, and onboard the ATMOSFER gondola aboard the ZPB. Datasets cover the altitude range from 4.5 to 9 km aboard the free release balloon and from 6 to 11.5 km aboard the ZPB. IWC values from both free release balloon and ZPB depict similar range, varying from ~1.10^{-5} to 0.015 g-m$^{-3,}$ with number concentration comprised between $2.4.10^{-3}$ and $2.5.10^{-2}$ cm^{-3}.

4.3.2 Stratospheric aerosols

Between 10.2 and 11.2 km, the NIXE-B measurements onboard the ZPB ATMOSFER show an additional layer with ice crystal area equivalent diameter of around 100 to 150 µm. No signature in ozone is observed in the vertical profiles of the ECC sondes, suggesting an airmass origin at high latitudes. The POPS and LPC instruments provided measurements of aerosols size distribution. Measurements during the ascent of the ZPB depicts an intense, thin layer of aerosols near 11 km, with diameters less than 0.5µm. Below this enriched layer, a highly depleted layer is observed between 9.3 and 10.2 km (see Fig. 9), which coincides with the altitude of large ice crystals and with the layer where a large vertical gradient of water vapor has been observed. Back trajectories initiated from a mean altitude of 9854 m, at the minimum of aerosol content. In the altitude range from 9.8 to 10.1 km, water vapor mixing ratio remains near 165.9 ppmv with a relative humidity over ice near 110 % and air temperature around -50°C. This layer extends up to the cold point tropopause.

Observations from Sentinel 5P (SP5) also show thin aerosol layers in the area from the East coast of Canada up to the Northwest of Russia on the day of flight. On the northeast coast of Labrador, in the sea of Labrador, a circular plume of aerosols, with UV index near 5.5 is observed by TROPOMI on SP5 on June 26, 2024. Isentropic airmass backward trajectories calculated from the balloon location show that the airmass intercepted the aerosol plume about a day before its sampling by the balloon borne instruments. SP5 observations estimate the mid-height of the aerosol plume between 10 and 12 km. The origin of the circular plume is not determined yet.

https://doi.org/10.5194/essd-2026-557
Preprint. Discussion started: 10 September 2026

4.3.2.1 Sub-tropical filament near 15.3 km

Between 14.5 and 16.7 km, a second layer of thin aerosols has been observed by the POPS particle counter, with particle diameters smaller than 0.2 µm and number concentrations of 1 to 5 cm^{-3}. This layer seems divided into two sublayers, one of 500 m thick near 15 km (420 K isentrope) with a number concentration of 5 cm^{-3} and a second layer near 16 km, with number concentration near 1 cm^{-3}. This double aerosol layer is correlated with a dry air (mixing ratio ~ 3.8 ppmv) and low ozone layer. The case of the isentrope near 420 K has been analyzed in section 4.2 using the MIMOSA model, tracing a potential origin of the higher aerosol density layer from the tropics. As for the second layer near 16km (435K isentrope), MIMOSA simulations suggest that the instruments have probed the external edge of the tropical filament, mixed with high latitude airmasses, thereby diluting the aerosol plume.

4.4 Assessment of radiances data

The evaluation of FIRMOS-B calibrated spectra was performed through a preliminary retrieval analysis using two independent radiative transfer and retrieval codes specifically designed for atmospheric FIR spectral radiance studies. The first code, KLIMA (Kyoto protocol Informed Management of the Adaptation), employs a line-by-line approach to simulate radiance under clear-sky conditions (Dinelli et al., 2023). The second code, FARM (FAst Retrieval Model), implements the fast retrieval scheme sigma-FORUM (Masiello et al., 2024) that enables the simulation of FIRMOS spectra within a few seconds by exploiting pre-computed optical depths, thus supporting all-sky conditions (Dinelli et al., 2022; Ridolfi et al., 2022). Both codes are versatile, allowing the analysis of measurements acquired in different geometrical configurations (limb, zenith, nadir for KLIMA and zenith, nadir for FARM) and across a broad spectral range, from millimetre and sub-millimetre wavelengths to the near infrared. They also enable the retrieval of atmospheric properties and instrumental parameters, including the Instrumental Spectral Response Function (ISRF). This approach provides a robust framework for assessing key performance indicators of FIRMOS measurements, i.e. the Noise Equivalent Spectral Radiance (NESR), the ISRF, and the Absolute Radiometric Accuracy (ARA).

All the quantities used for the data assessment are computed considering 200 spectra and selecting a subset of spectra that produce a final χ^2 below 2. This filtering criterion aims to retain clear-sky spectra that have been correctly processed.

The discrepancy between the simulated spectrum at the final iteration of the retrieval and the FIRMOS-B observations (i.e., the residuals) can be used to assess the accuracy of the NESR estimation. Specifically, the standard deviation of these residuals provides an a-posteriori estimate of the NESR. **Figure 13** illustrates this comparison by showing the standard deviation of the residuals (green line for KLIMA and blue line for FARM) alongside the averaged NESR for the considered measurements. The results indicate that the NESR is quantitatively consistent with the standard deviation of the residuals.

https://doi.org/10.5194/essd-2026-557
Preprint. Discussion started: 10 September 2026

Open Access Earth System Science Data Discussions

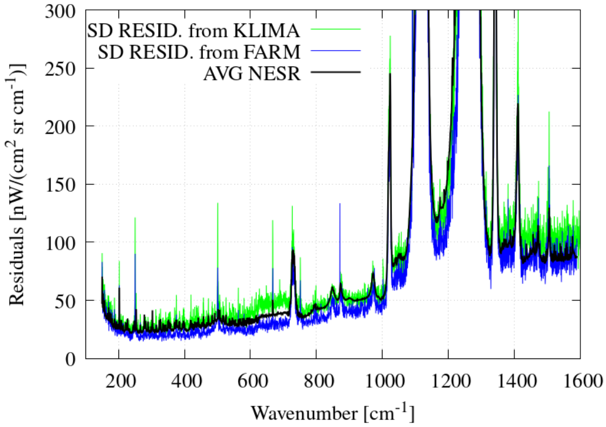

Figure 1**3**. Comparison between the standard deviation of the residuals and the averaged NESR (black line) for KLIMA (green line) and FARM (blue line).

The FIRMOS ISRF can be approximated by a linear combination of a sinc and sinc^2 functions to account for the field-of-view (FOV) aperture Ω as shown in the following equation:

$$ISRF = \alpha * \text{sinc}(2*L*\sigma) + (1-\alpha) * \text{sinc}^2(L*\sigma)$$

with the parameter α expressed as a function of Ω as

$$\alpha = \text{sinc}\,(L/2 * \sigma * \Omega)$$

where L is the maximum path difference, and σ is the nominal wavenumber of each channel.

The wavenumber can also be affected by scale factor error β, which depends on both Ω and potential drift of the reference laser. This error factor is evaluated during the quality control phase by fitting the wavenumber scale according to the relation:

$$\sigma' = (1 + \beta) * \sigma.$$

The reference laser exhibits a wavelength sensitivity of 0.059 nm/K. With the driver's thermal stability of 3-10 mK at 25 °C over 24 h, the expected maximum wavelength variation is about 0.00059 nm, corresponding to 1 ppm at 786 nm.

Figure 14 shows the frequency scale error β retrieved from the analysis by KLIMA and FARM, which are in close agreement. KLIMA reports an average shift of -0.3 ppm (retrieval error = 0.6 ppm; standard deviation (SD) = 0.8 ppm), while FARM gives 0.2 ppm (retrieval error = 0.6 ppm; SD: 0.8 ppm).

https://doi.org/10.5194/essd-2026-557
Preprint. Discussion started: 10 September 2026

Open Access Earth System Science Data Discussions

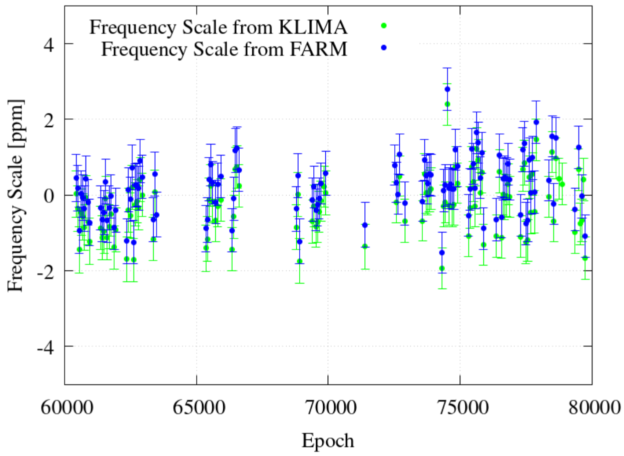

Figure 14. Frequency scale and retrieval error vs Epoch time retrieved by KLIMA (green points) and FARM (blue points).

Figure 15 shows the retrieved Ω values, also in this case in close agreement. KLIMA reports an average of 0.00088 sr (retrieval error = 0.00004 sr; SD = 0.0001 sr), while FARM obtains an average Ω of 0.00096 sr (retrieval error = 0.00003 sr; SD = 0.0001 sr).

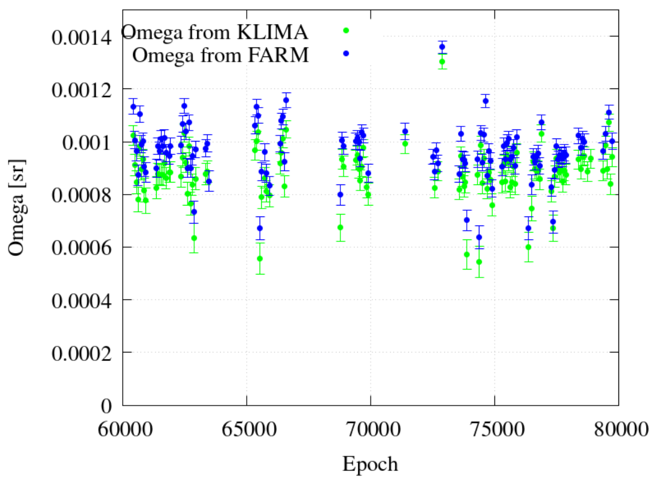

Figure 15. Retrieved omega (Ω) and retrieval error vs Epoch time retrieved by KLIMA (green points) and FARM (blue points).

The mean residuals between the simulated spectra at the last retrieval iteration and the FIRMOS-B measurements (residuals) can finally be used to perform an a-posteriori verification of the instrument ARA estimate, assuming the employed radiative transfer models do not introduce any simulation error. This latter assumption is supported by the extensive validation of both KLIMA and FARM with other datasets, particularly in the mid-infrared region above 650 cm^{-1} (Dinelli et al., 2023).

Figure 16 presents a comparison between the instrumental mean ARA and the average residuals (green line for KLIMA and blue line for FARM). For both codes, the magnitude of the average residuals falls within the ARA estimate, confirming the reliability of the estimate.

https://doi.org/10.5194/essd-2026-557
Preprint. Discussion started: 10 September 2026

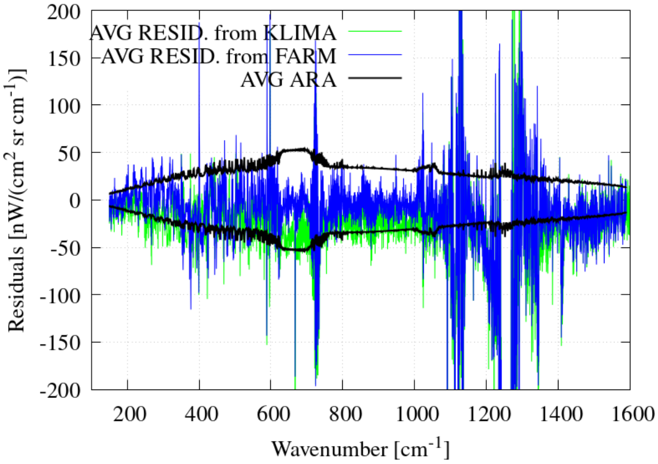

Figure 16. Comparison between the average of the residuals and the averaged ARA (black line) for KLIMA (green line) and FARM (blue line).

During the retrieval analysis, the following atmospheric parameters were derived: vertical profiles of temperature, water vapor, ozone, and cloud properties (e.g., IWC and effective radius). Additionally, surface temperature and emissivity were also retrieved. A comprehensive discussion of these results exceeds the scope of this paper and will be addressed in a forthcoming publication. **Figure 17** presents an example of the retrieved vertical profiles of temperature and water vapor compared with the radiosonde measurements.

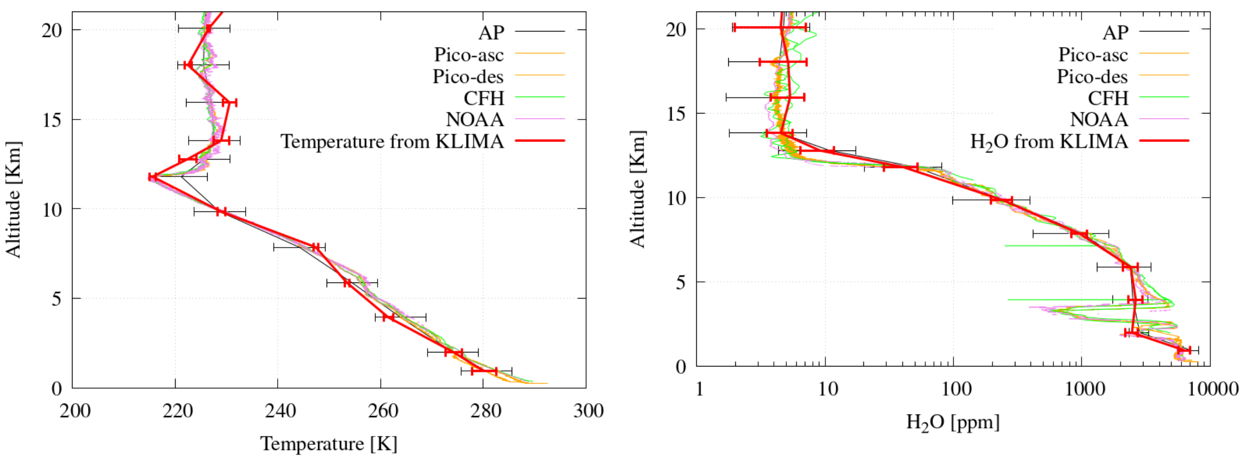

Figure 17. Example of retrieved temperature and water vapor profiles (red line) compared with radiosonde observations performed with Pico-Light, CFH, and NOAA FPH. AP is the a priori profile from ERA 5 used as initial guess.

The comparison of FIRMOS-B retrievals with in situ profiles will be discussed in detail in a forthcoming paper. Nevertheless, a first comparison shows a good agreement in the tropospheric part of the profiles (i.e. for altitudes below 10 km). Discrepancies can be observed in the stratospheric part of the profile, especially near 12 and 16 km, altitudes where aerosol layers and optically thin cirrus near the tropopause were found. Further analysis will investigate the role of aerosol layers in these discrepancies.

Such a result is encouraging and further analysis is ongoing to evaluate and validate FORUM-like observations.

Conclusions

The ATMOSFER campaign took place from the Esrange Space Center in Kiruna, Sweden on June 26-27, 2024. This field campaign aimed to perform preparation activities of the upcoming ESA FORUM mission. During the ZPB flight which lasted about 11 hours, atmospheric conditions were highly variable, with the tropopause height changing by close to 1km.

The data collected include vertical profiles of water vapor from 3 different hygrometers (Pico-Light H_2O, FPH and CFH), particle size distribution (from OPCs: POPS, LOAC1.5, LPC and NIXE-B), ice crystal size and shape (NIXE-B imager), ozone (ECC ozone sonde) and far infrared radiances from the balloon-borne demonstrator of the ESA FORUM instrument (FIRMOS-B instrument).

The analysis of balloon borne data shows that cirrus clouds were sampled between 6 and 11 km, for which size and shape distribution could be retrieved. The IWC and crystal number concentration were retrieved from NIXE-B measurements aboard free-release balloon and ZPB during the ascent of the balloons. Relative humidities over ice from 100 to 137% were measured inside the cloud. The cirrus was observed in presence of aerosols of size below 450 nm. A layer of larger particles (2 to 3 µm) was observed near 8 km. Ensemble back-trajectories were calculated using the HYSPLIT model to trace back the origin of the aerosol plume. This thick layer of aerosols most probably originates from Canadian wildfires with events occurring from May 9 to June 25. Layer of stratospheric aerosols were also observed near 11 and 15 km, originating respectively from an aerosol plume of high aerosol index (5.5) observed by TROPOMI aboard SP5 a day before the flight over the Labrador Sea and from the intrusion of a tropical filament.

The assessment of far infrared spectral radiances measured by the FIRMOS-B instrument using the complementary information brought by in situ hygrometers and particle counters will allow to evaluate the quality of the retrievals and to raise questions on the influence of aerosols and optically thin cirrus on the far-infrared retrievals of FORUM-like observations. Such a deeper analysis will be the subject of a forthcoming paper.

Data availability

FIRMOS-B dataset is available via the ESA campaign dataset website https://earth.esa.int/eogateway/campaigns/firmos (.... doi still to be assigned ...). Pico-Light, NOAA FPH, CFH, POPS, LOAC and NIXE-B datasets are available for access on the AERIS/DATA TERRA datacenter:

Instrument	Date	DOI
Pico-Light H_2O	2024-06-26 23:50:23 UTC => 2024-06-27 00:15:17 UTC	*https://doi.org/10.25326/ECTJ-5787*

https://doi.org/10.5194/essd-2026-557
Preprint. Discussion started: 10 September 2026

	2024-06-27 01:26:38 UTC => 2024-06-27 01:52:39 UTC	*https://doi.org/10.25326/H663-SZ56*
	2024-06-27 08:37:53 UTC => 2024-06-27 09:11:05 UTC	*https://doi.org/10.25326/ZNM5-9S13*
	2024-06-27 10:04:00 UTC => 2024-06-27 10:53:34 UTC	*https://doi.org/10.25326/M78G-AD37*
NOAA FPH	2024-06-27 00:08:07 UTC => 2024-06-27 02:08:07 UTC	*https://doi.org/10.25326/GJ6Y-ZZ25*
	2024-06-27 08:38:53 UTC => 2024-06-27 10:38:07 UTC	*https://doi.org/10.25326/EY6D-B587*
CFH	2024-06-27 00:07:26 UTC => 2024-06-27 02:07:26 UTC	*https://doi.org/10.25326/HERQ-MJ06*
	2024-06-27 08:39:34 UTC => 2024-06-27 10:38:07 UTC	*https://doi.org/10.25326/C9XP-SZ76*
LOAC v1.5	2024-06-26 23:02:10 UTC => 2024-06-27 00:54:56 UTC	*https://doi.org/10.25326/NC3N-3457*
POPS	2024-06-26 23:02:10 UTC => 2024-06-27 00:54:56 UTC	*https://doi.org/10.25326/D8X8-QB98*
NIXE-B	2024-06-27 00:22:13 UTC => 2024-06-27 00:34:22 UTC	*https://doi.org/10.25326/85C5-CZ07*
	2024-06-27 00:22:13 UTC => 2024-06-27 00:34:22 UTC	*https://doi.org/10.25326/AXEG-Y934*
	2024-06-26 23:13:50 UTC => 2024-06-26 23:24:13 UTC	*https://doi.org/10.25326/3P0D-YN06*
	2024-06-26 23:13:50 UTC => 2024-06-26 23:24:13 UTC	*https://doi.org/10.25326/NQ32-ZP98*
LPC	2024-06-26 23:02:10 UTC => 2024-06-27 00:54:56 UTC	*https://doi.org/10.25326/FY0M-4J44*

A single link will be created to access the full dataset.

Author contributions

M.G. coordinated the ATMOSFER campaign, M.G and G.D processed Pico-Light H_2O data, N.A., J.-C.S., prepared the Pico-Light instrument for flights. A.H. contributed in the airmass transport modelling (MIMOSA expertise and PV fields); G.B. provided the LOAC and POPS instruments, analyzed the balloon-borne aerosol data. L.P., C.B., S.V., and M.B. contributed to the preparation and execution of the ATMOSFER field campaign. They were responsible for the integration, pre-flight testing, and operation of the FIRMOS-B instrument during the airborne measurements, as well as for the processing and analysis of the acquired data. P.P. and S.D.B. performed quality assessment and validation of the FIRMOS-B measurements and carried out the retrieval of atmospheric state parameters, including water vapour and temperature profiles, together with cloud property retrievals. E.A., E.H., A.F. provided the FPH instruments and FPH data for the paper. C.R. provided the CFH hygrometer and the CFH data for the paper. L.K. and T.D. provided the LPC instrument, analyzed the data for presentation in the paper in the same style as the other OPCs. T.K., C.S., A.A. developed and prepared the NIXE-B instrument. A.A. was PI for NIXE-B provided the analysed data. All coauthors contributed to the final revision of the manuscript.

Acknowledgements

We thank N. Le Tohic, J. Edman, B. Bocquet, E. Storbacka and E. Lundquist of the SSC Space for their reactivity in replying to our request during the in-field campaign and the great support they provided on site and in the process of flight authorizations for the CFH, NIXE-B and FPH free-release balloon flights. The authors gratefully acknowledge Dr. Dirk Schüttemeyer and Dr. Hilke Oetjen for their continuous support to the FIRMOS programme through the funding and coordination of FORUM preparatory activities, in their respective roles as ESA FORUM Mission Scientist and Scientific Campaign Coordinator.

Financial support

This research and the campaign participation were funded by CNES balloon program for Pico-Light, POPS, LOAC instruments, and by the FIRMOS–Balloon—Technical Assistance for a Far-Infrared Radiation airborne Observation System (EE9 Forum) Project, ESA Contract No. 4000137321/22/NL/AD. Support for the LPC participation was funded by the US National Science Foundation under award 1745008.

References

Asher, E., Baron, A., Yu, P., Todt, M., Smale, P., Liley, B., Querel, R., Sakai, T., Morino, I., Jin, Y., Nagai, T., Uchino, O., Hall, E., Cullis, P., Johnson, B., and Thornberry, T. D.: Balloon Baseline Stratospheric Aerosol Profiles (B2SAP)—Perturbations in the Southern Hemisphere, 2019–2022, Journal of Geophysical Research: Atmospheres, 129, e2024JD041581, https://doi.org/10.1029/2024JD041581, 2024.

Banerjee, A., Chiodo, G., Previdi, M., Ponater, M., Conley, A. J., and Polvani, L. M.: Stratospheric water vapor: an important climate feedback, Clim Dyn, 53, 1697–1710, https://doi.org/10.1007/s00382-019-04721-4, 2019.

Belotti, C., Barbara, F., Barucci, M., Bianchini, G., D'Amato, F., Del Bianco, S., Di Natale, G., Gai, M., Montori, A., Pratesi, F., Rettinger, M., Rolf, C., Sussmann, R., Trickl, T., Viciani, S., Vogelmann, H., and Palchetti, L.: The Far-Infrared Radiation Mobile Observation System (FIRMOS) for spectral characterization of the atmospheric emission, Atmospheric Measurement Techniques, 16, 2511–2529, https://doi.org/10.5194/amt-16-2511-2023, 2023.

Brunamonti, S., Saathoff, H., Hertzog, A., Diskin, G., Fujiwara, M., Rosenlof, K., Möhler, O., Tuzson, B., Emmenegger, L., Amarouche, N., Durry, G., Frérot, F., Samake, J.-C., Cenac, C., Lopez, J., Monnier, P., and Ghysels, M.: The AquaVIT-4 intercomparison of atmospheric hygrometers, Atmospheric Measurement Techniques, 18, 5321–5348, https://doi.org/10.5194/amt-18-5321-2025, 2025.

Charlesworth, E., Plöger, F., Birner, T., Baikhadzhaev, R., Abalos, M., Abraham, N. L., Akiyoshi, H., Bekki, S., Dennison, F., Jöckel, P., Keeble, J., Kinnison, D., Morgenstern, O., Plummer, D., Rozanov, E., Strode, S., Zeng, G., Egorova, T., and Riese, M.: Stratospheric water vapor affecting atmospheric circulation, Nat Commun, 14, 3925, https://doi.org/10.1038/s41467-023-39559-2, 2023.

Deshler, T. and Kalnajs, L. E.: Ratios of Extinction Coefficient, Mass, and Surface Area to Backscatter Coefficient and Mass to Extinction Coefficient Derived From Balloon-Borne Stratospheric Aerosol Size Distribution Measurements From 1989–2025, Journal of Geophysical Research: Atmospheres, 131, e2025JD045262, https://doi.org/10.1029/2025JD045262, 2026.

Deshler, T., Kalnajs, L. E., Norgren, M., Zhu, Y., and Zhang, J.: In Situ Aerosol Size Spectra Measurements in the Austral Polar Vortex Before and After the Hunga Tonga-Hunga Ha'apai Volcanic Eruption, Geophysical Research Letters, 51, e2024GL111388, https://doi.org/10.1029/2024GL111388, 2024.

Dessler, A. E.: Observations of Climate Feedbacks over 2000–10 and Comparisons to Climate Models, J. Climate, 26, 333–342, https://doi.org/10.1175/JCLI-D-11-00640.1, 2013.

Dessler, A. E., Schoeberl, M. R., Wang, T., Davis, S. M., and Rosenlof, K. H.: Stratospheric water vapor feedback, PNAS, 110, 18087–18091, https://doi.org/10.1073/pnas.1310344110, 2013.

Dessler, A. E., Schoeberl, M. R., Wang, T., Davis, S. M., Rosenlof, K. H., and Vernier, J.-P.: Variations of stratospheric water vapor over the past three decades, Journal of Geophysical Research: Atmospheres, 119, 12,588-12,598, https://doi.org/https://doi.org/10.1002/2014JD021712, 2014.

Dinelli, B. M., Ridolfi, M., Masiello, G., Serio, C., Venafra, S, Maestri, T., Del Bianco, S, Raspollini, P, Lorenzi, G, and Palchetti, L: A Fast Retrieval Model for the Inversion of Surface, Atmospheric and Cloud properties from Nadir FIR and TIR measurements, in: In Proceedings of the Living Planet Symposium, 2022.

Dinelli, B. M., Del Bianco, S., Castelli, E., Di Roma, A., Lorenzi, G., Premuda, M., Barbara, F., Gai, M., Raspollini, P., and Di Natale, G.: GBB-Nadir and KLIMA: Two Full Physics Codes for the Computation of the Infrared Spectrum of the Planetary Radiation Escaping to Space, Remote Sensing, 15, 2532, https://doi.org/10.3390/rs15102532, 2023.

Eyring, V., Butchart, N., Waugh, D. W., Akiyoshi, H., Austin, J., Bekki, S., Bodeker, G. E., Boville, B. A., Brühl, C., Chipperfield, M. P., Cordero, E., Dameris, M., Deushi, M., Fioletov, V. E., Frith, S. M., Garcia, R. R., Gettelman, A., Giorgetta, M. A., Grewe, V., Jourdain, L., Kinnison, D. E., Mancini, E., Manzini, E., Marchand, M., Marsh, D. R., Nagashima, T., Newman, P. A., Nielsen, J. E., Pawson, S., Pitari, G., Plummer, D. A., Rozanov, E., Schraner, M., Shepherd, T. G., Shibata, K., Stolarski, R. S., Struthers, H., Tian, W., and Yoshiki, M.: Assessment of temperature, trace species, and ozone in chemistry-climate model simulations of the recent past, Journal of Geophysical Research: Atmospheres, 111, https://doi.org/10.1029/2006JD007327, 2006.

Gao, R. S., Telg, H., McLaughlin, R. J., Ciciora, S. J., Watts, L. A., Richardson, M. S., Schwarz, J. P., Perring, A. E., Thornberry, T. D., Rollins, A. W., Markovic, M. Z., Bates, T. S., Johnson, J. E., and Fahey, D. W.: A light-weight, high-sensitivity particle spectrometer for PM2.5 aerosol measurements, Aerosol Science and Technology, 50, 88–99, https://doi.org/10.1080/02786826.2015.1131809, 2016.

Ghysels, M., Durry, G., Amarouche, N., Hurst, D., Hall, E., Xiong, K., Dupont, J.-C., Samake, J.-C., Frérot, F., Bejjani, R., and Riviere, E. D.: Pico-Light H_2O: intercomparison of in situ water vapor measurements during the AsA 2022 campaign, Atmospheric Measurement Techniques, 17, 3495–3513, https://doi.org/10.5194/amt-17-3495-2024, 2024.

Hall, E. G., Jordan, A. F., Hurst, D. F., Oltmans, S. J., Vömel, H., Kühnreich, B., and Ebert, V.: Advancements, measurement uncertainties, and recent comparisons of the NOAA frost point hygrometer, Atmos. Meas. Tech., 9, 4295–4310, https://doi.org/10.5194/amt-9-4295-2016, 2016.

Hauchecorne, A., Godin, S., Marchand, M., Heese, B., and Souprayen, C.: Quantification of the transport of chemical constituents from the polar vortex to midlatitudes in the lower stratosphere using the high-resolution advection model MIMOSA and effective diffusivity, Journal of Geophysical Research: Atmospheres, 107, SOL 32-13, https://doi.org/10.1029/2001JD000491, 2002.

https://doi.org/10.5194/essd-2026-557
Preprint. Discussion started: 10 September 2026

Hegglin, M. I., Plummer, D. A., Shepherd, T. G., Scinocca, J. F., Anderson, J., Froidevaux, L., Funke, B., Hurst, D., Rozanov, A., Urban, J., von Clarmann, T., Walker, K. A., Wang, H. J., Tegtmeier, S., and Weigel, K.: Vertical structure of stratospheric water vapor trends derived from merged satellite data, Nat Geosci, 7, 768–776, https://doi.org/10.1038/ngeo2236, 2014.

Hurst, D. F., Hall, E. G., Jordan, A. F., Miloshevich, L. M., Whiteman, D. N., Leblanc, T., Walsh, D., Vömel, H., and Oltmans, S. J.: Comparisons of temperature, pressure and humidity measurements by balloon-borne radiosondes and frost point hygrometers during MOHAVE-2009, Atmos. Meas. Tech., 4, 2777–2793, https://doi.org/10.5194/amt-4-2777-2011, 2011a.

Hurst, D. F., Oltmans, S. J., Vömel, H., Rosenlof, K. H., Davis, S. M., Ray, E. A., Hall, E. G., and Jordan, A. F.: Stratospheric water vapor trends over Boulder, Colorado: Analysis of the 30 year Boulder record, Journal of Geophysical Research: Atmospheres, 116, https://doi.org/10.1029/2010JD015065, 2011b.

Hurst, D. F., Read, W. G., Vömel, H., Selkirk, H. B., Rosenlof, K. H., Davis, S. M., Hall, E. G., Jordan, A. F., and Oltmans, S. J.: Recent divergences in stratospheric water vapor measurements by frost point hygrometers and the Aura Microwave Limb Sounder, Atmos. Meas. Tech., 9, 4447–4457, https://doi.org/10.5194/amt-9-4447-2016, 2016.

Immler, F. J., Dykema, J., Gardiner, T., Whiteman, D. N., Thorne, P. W., and Vömel, H.: Reference Quality Upper-Air Measurements: guidance for developing GRUAN data products, Atmospheric Measurement Techniques, 3, 1217–1231, https://doi.org/10.5194/amt-3-1217-2010, 2010.

Kalnajs, L. E. and Deshler, T.: A New Instrument for Balloon-Borne In Situ Aerosol Size Distribution Measurements, the Continuation of a 50 Year Record of Stratospheric Aerosols Measurements, Journal of Geophysical Research: Atmospheres, 127, e2022JD037485, https://doi.org/10.1029/2022JD037485, 2022.

Keeble, J., Hassler, B., Banerjee, A., Checa-Garcia, R., Chiodo, G., Davis, S., Eyring, V., Griffiths, P. T., Morgenstern, O., Nowack, P., Zeng, G., Zhang, J., Bodeker, G., Burrows, S., Cameron-Smith, P., Cugnet, D., Danek, C., Deushi, M., Horowitz, L. W., Kubin, A., Li, L., Lohmann, G., Michou, M., Mills, M. J., Nabat, P., Olivié, D., Park, S., Seland, Ø., Stoll, J., Wieners, K.-H., and Wu, T.: Evaluating stratospheric ozone and water vapor changes in CMIP6 models from 1850 to 2100, Atmospheric Chemistry and Physics, 21, 5015–5061, https://doi.org/10.5194/acp-21-5015-2021, 2021.

Khordakova, D., Rolf, C., Grooß, J.-U., Müller, R., Konopka, P., Wieser, A., Krämer, M., and Riese, M.: A case study on the impact of severe convective storms on the water vapor mixing ratio in the lower mid-latitude stratosphere observed in 2019 over Europe, Atmospheric Chemistry and Physics, 22, 1059–1079, https://doi.org/10.5194/acp-22-1059-2022, 2022.

Kloss, C., Sellitto, P., Legras, B., Vernier, J.-P., Jégou, F., Venkat Ratnam, M., Suneel Kumar, B., Lakshmi Madhavan, B., and Berthet, G.: Impact of the 2018 Ambae Eruption on the Global Stratospheric Aerosol Layer and Climate, Journal of Geophysical Research: Atmospheres, 125, e2020JD032410, https://doi.org/10.1029/2020JD032410, 2020.

Konopka, P., Tao, M., Ploeger, F., Hurst, D. F., Santee, M. L., Wright, J. S., and Riese, M.: Stratospheric Moistening After 2000, Geophysical Research Letters, 49, e2021GL097609, https://doi.org/10.1029/2021GL097609, 2022.

Kuhn, T. and Heymsfield, A. J.: In Situ Balloon-Borne Ice Particle Imaging in High-Latitude Cirrus, Pure Appl. Geophys., 173, 3065–3084, https://doi.org/10.1007/s00024-016-1324-x, 2016.

Lait, L. R.: An Alternative Form for Potential Vorticity, Journal of the Atmospheric Sciences, 51, 1754–1759, https://doi.org/10.1175/1520-0469(1994)051%3C1754:AAFFPV%3E2.0.CO;2, 1994.

Masiello, G., Serio, C., Maestri, T., Martinazzo, M., Masin, F., Liuzzi, G., and Venafra, S.: The new σ-IASI code for all sky radiative transfer calculations in the spectral range 10 to 2760 cm-1: σ-IASI/F2N, Journal of Quantitative Spectroscopy and Radiative Transfer, 312, 108814, https://doi.org/10.1016/j.jqsrt.2023.108814, 2024.

Müller, R., Kunz, A., Hurst, D. F., Rolf, C., Krämer, M., and Riese, M.: The need for accurate long-term measurements of water vapor in the upper troposphere and lower stratosphere with global coverage, Earth's Future, 4, 25–32, https://doi.org/10.1002/2015EF000321, 2016.

Nowack, P., Ceppi, P., Davis, S. M., Chiodo, G., Ball, W., Diallo, M. A., Hassler, B., Jia, Y., Keeble, J., and Joshi, M.: Response of stratospheric water vapor to warming constrained by satellite observations, Nat. Geosci., 16, 577–583, https://doi.org/10.1038/s41561-023-01183-6, 2023.

Oltmans, S. J., Vömel, H., Hofmann, D. J., Rosenlof, K. H., and Kley, D.: The increase in stratospheric water vapor from balloonborne, frostpoint hygrometer measurements at Washington, D.C., and Boulder, Colorado, Geophys. Res. Lett., 27, 3453–3456, https://doi.org/10.1029/2000GL012133, 2000.

Palchetti, L., Barucci, M., Belotti, C., Bianchini, G., Cluzet, B., D'Amato, F., Del Bianco, S., Di Natale, G., Gai, M., Khordakova, D., Montori, A., Oetjen, H., Rettinger, M., Rolf, C., Schuettemeyer, D., Sussmann, R., Viciani, S., Vogelmann, H., and Wienhold, F. G.: Observations of the downwelling far-infrared atmospheric emission at the Zugspitze observatory, Earth System Science Data, 13, 4303–4312, https://doi.org/10.5194/essd-13-4303-2021, 2021.

Renard, J.-B., Dulac, F., Berthet, G., Lurton, T., Vignelles, D., Jégou, F., Tonnelier, T., Jeannot, M., Couté, B., Akiki, R., Verdier, N., Mallet, M., Gensdarmes, F., Charpentier, P., Mesmin, S., Duverger, V., Dupont, J.-C., Elias, T., Crenn, V., Sciare, J., Zieger, P., Salter, M., Roberts, T., Giacomoni, J., Gobbi, M., Hamonou, E., Olafsson, H., Dagsson-Waldhauserova, P., Camy-Peyret, C., Mazel, C., Décamps, T., Piringer, M., Surcin, J., and Daugeron, D.: LOAC: a small aerosol optical counter/sizer for ground-based and balloon measurements of the size distribution and nature of atmospheric particles – Part 2: First results from balloon and unmanned aerial vehicle flights, Atmospheric Measurement Techniques, 9, 3673–3686, https://doi.org/https://doi.org/10.5194/amt-9-3673-2016, 2016.

Ridolfi, M., Tirelli, C., Ceccherini, S., Belotti, C., Cortesi, U., and Palchetti, L.: Synergistic retrieval and complete data fusion methods applied to simulated FORUM and IASI-NG measurements, Atmospheric Measurement Techniques, 15, 6723–6737, https://doi.org/10.5194/amt-15-6723-2022, 2022.

Rosenlof, K. H., Oltmans, S. J., Kley, D., Russell, J. M., Chiou, E.-W., Chu, W. P., Johnson, D. G., Kelly, K. K., Michelsen, H. A., Nedoluha, G. E., Remsberg, E. E., Toon, G. C., and McCormick, M. P.: Stratospheric water vapor increases over the past half-century, Geophys. Res. Lett., 28, 1195–1198, https://doi.org/10.1029/2000GL012502, 2001.

Smith, H. R., Ulanowski, Z., Kaye, P. H., Hirst, E., Stanley, W., Kaye, R., Wieser, A., Stopford, C., Kezoudi, M., Girdwood, J., Greenaway, R., and Mackenzie, R.: The Universal Cloud and Aerosol Sounding System (UCASS): a low-cost miniature optical particle counter for use in dropsonde or balloon-borne sounding systems, Atmospheric Measurement Techniques, 12, 6579–6599, https://doi.org/10.5194/amt-12-6579-2019, 2019.

Solomon, S., Rosenlof, K. H., Portmann, R. W., Daniel, J. S., Davis, S. M., Sanford, T. J., and Plattner, G.-K.: Contributions of Stratospheric Water Vapor to Decadal Changes in the Rate of Global Warming, Science, 327, 1219–1223, https://doi.org/10.1126/science.1182488, 2010.

Tao, M., Konopka, P., Wright, J. S., Liu, Y., Bian, J., Davis, S. M., Jia, Y., and Ploeger, F.: Multi-decadal variability controls short-term stratospheric water vapor trends, Commun Earth Environ, 4, 441, https://doi.org/10.1038/s43247-023-01094-9, 2023.

Todt, M. A., Asher, E., Hall, E., Cullis, P., Jordan, A., Xiong, K., Hurst, D. F., and Thornberry, T.: Baseline Balloon Stratospheric Aerosol Profiles (B2SAP)—Systematic Measurements of Aerosol Number Density and Size, Journal of Geophysical Research: Atmospheres, 128, e2022JD038041, https://doi.org/10.1029/2022JD038041, 2023.

https://doi.org/10.5194/essd-2026-557
Preprint. Discussion started: 10 September 2026

Vömel, H., David, D. E., and Smith, K.: Accuracy of tropospheric and stratospheric water vapor measurements by the cryogenic frost point hygrometer: Instrumental details and observations, J. Geophys. Res., 112, D08305, https://doi.org/10.1029/2006JD007224, 2007.

Vömel, H., Naebert, T., Dirksen, R., and Sommer, M.: An update on the uncertainties of water vapor measurements using cryogenic frost point hygrometers, Atmospheric Measurement Techniques, 9, 3755–3768, https://doi.org/10.5194/amt-9-3755-2016, 2016.